LBL-36149
UC-364

Lawrence Berkeley Laboratory

UNIVERSITY OF CALIFORNIA

ENERGY & ENVIRONMENT DIVISION

Ion-Assisted Laser Deposition of Intermediate Layers for $YBa_2Cu_3O_{7-\delta}$ Thin Film Growth on Polycrystalline and Amorphous Substrates

R.P. Reade
(Ph.D. Thesis)

November 1993

ENERGY & ENVIRONMENT DIVISION

REFERENCE COPY
Does Not
Circulate
Bldg. 50 Library.
LBL-36149
Copy 1

Prepared for the U.S. Department of Energy under Contract Number DE-AC03-76SF00098

DISCLAIMER

This document was prepared as an account of work sponsored by the United States Government. While this document is believed to contain correct information, neither the United States Government nor any agency thereof, nor The Regents of the University of California, nor any of their employees, makes any warranty, express or implied, or assumes any legal responsibility for the accuracy, completeness, or usefulness of any information, apparatus, product, or process disclosed, or represents that its use would not infringe privately owned rights. Reference herein to any specific commercial product, process, or service by its trade name, trademark, manufacturer, or otherwise, does not necessarily constitute or imply its endorsement, recommendation, or favoring by the United States Government or any agency thereof, or The Regents of the University of California. The views and opinions of authors expressed herein do not necessarily state or reflect those of the United States Government or any agency thereof, or The Regents of the University of California.

Lawrence Berkeley Laboratory is an equal opportunity employer.

DISCLAIMER

This document was prepared as an account of work sponsored by the United States Government. While this document is believed to contain correct information, neither the United States Government nor any agency thereof, nor the Regents of the University of California, nor any of their employees, makes any warranty, express or implied, or assumes any legal responsibility for the accuracy, completeness, or usefulness of any information, apparatus, product, or process disclosed, or represents that its use would not infringe privately owned rights. Reference herein to any specific commercial product, process, or service by its trade name, trademark, manufacturer, or otherwise, does not necessarily constitute or imply its endorsement, recommendation, or favoring by the United States Government or any agency thereof, or the Regents of the University of California. The views and opinions of authors expressed herein do not necessarily state or reflect those of the United States Government or any agency thereof or the Regents of the University of California.

LBL-36149
UC-364

ION-ASSISTED LASER DEPOSITION OF INTERMEDIATE LAYERS FOR $YBa_2Cu_3O_{7-\delta}$ THIN FILM GROWTH ON POLYCRYSTALLINE AND AMORPHOUS SUBSTRATES

by

Ronald P. Reade
Ph.D. Thesis

Department of Materials Science and Mineral Engineering
University of California

and

Energy & Environment Division
Lawrence Berkeley Laboratory
Berkeley, California 94720

November 1993

This work was supported by the Advanced Research Projects Agency (ARPA) and by the Assistant Secretary for Energy Efficiency and Renewable Energy, Office of Energy Management, Advanced Utility Concepts Division of the U.S. Department of Energy under Contract No. DE-AC03-76SF00098.

Abstract

Ion-Assisted Laser Deposition of Intermediate Layers for $YBa_2Cu_3O_{7-\delta}$ Thin Film Growth on Polycrystalline and Amorphous Substrates

by

Ronald Paul Reade

Doctor of Philosophy in Materials Science
and Mineral Engineering

University of California at Berkeley

Professor Eugene E. Haller, Chair

The growth of $YBa_2Cu_3O_{7-\delta}$ (YBCO) high-temperature superconductor thin films has largely been limited to deposition on single-crystal substrates to date. In order to expand the range of potential applications, growth on polycrystalline and amorphous substrates is desirable. In particular, the deposition of YBCO thin films with high critical current densities on polycrystalline metal alloys would allow the

manufacture of superconducting tapes. However, it is shown that it is not possible to grow YBCO thin films directly on this type of substrate due to chemical and structural incompatibility. This work investigates the use of a yttria-stabilized zirconia (YSZ) intermediate layer to address this problem. An ion-assisted pulsed-laser deposition process is developed to provide control of orientation during the growth of the YSZ layers.

The important properties of YBCO and YSZ are summarized and the status of research on thin film growth of these materials is reviewed. An overview of the pulsed-laser deposition (PLD) technique is presented. The use of ion-assisted deposition techniques to control thin film properties is discussed.

Using an ion-assisted PLD process, the growth of (001) YSZ layers with controlled alignment of the in-plane crystal axes is achieved on polycrystalline metal and other polycrystalline and amorphous substrates.. Studies of the important process parameters are presented. These layers are demonstrated to be appropriate for the subsequent deposition of *c*-axis YBCO thin films with alignment of the in-plane axes. A critical temperature of 92K and critical current densities (at 77K) of $6x10^5$ and $5x10^4$ A/cm^2, without and with a 0.4T

magnetic field, have been achieved. These critical current densities are higher than those demonstrated for competing technologies.

The applicability of the developed technology is discussed. The control of film orientation using the ion-assisted PLD process is compared to the existing theory and shown to be in agreement. This is the first demonstrated use of ion-assisted orientation control in conjunction with PLD.

(11/18/93)

TABLE OF CONTENTS

1. Introduction/High Temperature Superconductors 1

2. $YBa_2Cu_3O_{7-\delta}$ Thin Films 4

2.1. $YBa_2Cu_3O_{7-\delta}$ properties 4

2.2. Epitaxial films 11

2.2.1. Growth on compatible substrates 11

2.2.2. Growth on incompatible substrates using intermediate layers 12

2.3. Non-epitaxial films/use of intermediate layers 14

3. Yttria-Stabilized Zirconia (YSZ) Thin Films 16

3.1. YSZ properties/use in other technologies 16

3.2. Use as intermediate layer for $YBa_2Cu_3O_{7-\delta}$ thin film growth 21

4. Pulsed-Laser Deposition Overview 23

4.1. Pulsed-Laser Deposition Concept 23

4.2. Advantages for Thin Film Growth 27

5. Ion-Assisted Thin Film Growth 30

5.1. Modification of film properties 32

5.2. Control of thin film orientation 34

5.2.1. Previous studies 34

5.2.2. Theory 37

6. Experimental 39

6.1. Pulsed-laser deposition 39

6.1.1. System overview 39

6.1.2. Typical deposition procedures and conditions 44

6.2. Materials specification and preparation 47

6.2.1. Substrates 47

6.2.1.1. Haynes Alloy #230 47

6.2.1.2. Other substrates 49

6.2.2. Targets 49

6.3. Characterization techniques 50

6.3.1. X-ray Diffraction 50

6.3.1.1. 2θ diffraction 50

6.3.1.2. ϕ-scans and rocking curves 52

6.3.2. Electrical measurements 54

6.3.2.1. Resistance vs temperature 54

6.3.2.1. Critical current density 57

6.3.3. Other techniques 57

7. Results 60

7.1. $YBa_2Cu_3O_{7-\delta}$ deposition on $SrTiO_3$ for process definition 60

7.1.1. Process parameters 60

7.1.2. Film characterization 62

7.2. $YBa_2Cu_3O_{7-\delta}$ deposition directly on Haynes Alloy #230 66

7.3. YSZ deposition on Haynes Alloy #230 70
7.3.1. Non-ion-assisted deposition 70
7.3.1.1. Temperature effects 71
7.3.1.2. Pressure effects 72
7.3.1.3. Suitability of layers for $YBa_2Cu_3O_{7-\delta}$ growth 74
7.3.2. Ion-assisted deposition 79
7.3.2.1. Orientation control 80
7.3.2.2. Ar^+ vs. O_2^+ effects 82
7.3.2.3. Beam voltage effects 83
7.3.2.4. Beam current effects 86
7.3.3. Deposition on other substrates 87
7.4. $YBa_2Cu_3O_{7-\delta}$ deposition on YSZ/Haynes Alloy #230 89

8. Discussion 95
8.1. $YBa_2Cu_3O_{7-\delta}$ results and potential 95
8.2. Applicability of demonstrated technology 97
8.3. Mechanism of YSZ orientation control by ion-assisted pulsed-laser deposition 100
8.4. Suggestions for future research 105

9. References 108

ACKNOWLEDGEMENTS

In the course of my studies, I have been helped, supported, and encouraged by many people. First, I would like to express my deepest gratitude to Richard E. Russo and Eugene E. Haller for their guidance, patience, and the occasional kick-in-the-behind when I needed it most. It has been a pleasure and a privilege to work with both of you and your talented groups.

Next, I must thank several people with whom I have worked. Paul Berdahl helped me with many of the electrical measurements that are contained in this work, and always had an open door when I had a question. Xianglei Mao contributed to the YSZ process investigations. Stefan Church created amazing Claris-CAD designs, and lent a hand in the lab when he wasn't in the machine shop. Steve Garrison of Conductus, Inc. assisted with x-ray measurements. Barry Olsen of the Lawrence Livermore Laboratory lent his mechanical expertise during the building of the vacuum system. It has been a pleasure to work with everyone.

I am indebted to the two research groups of which I have been a part. It has been a blast to be a member of the Team Destructo laser group. The Lawrence Berkeley Laboratory Electronic Materials

Group always provided worthwhile advice. In particular, I thank my fellow graduate students for their help in getting me through grad. school.

Thank you to Prof. Cheung, for reading this manuscript in a timely manner.

I would like to express my appreciation to all of my friends who have supported me outside of my graduate work. Also, my thanks go to the Cal Cycling Team for keeping me sane during grad. school.

Finally, my gratitude to everyone in my family for constantly being behind me. In particular, I thank my uncle, Joseph Bernick, who has always looked out for my future.

1. INTRODUCTION/HIGH TEMPERATURE SUPERCONDUCTORS

In 1986, J. G. Bednorz and K. A. Müller [1] started a new era of superconductivity research with the announcement of superconductivity at a temperature of ~30 K in $La_{2-x}Ba_xCuO_{4-\delta}$. Within a year, superconductivity at ~ 90 K, well above the boiling point of liquid nitrogen (77 K), was demonstrated for the $YBa_2Cu_3O_{7-\delta}$ compound [2]. These discoveries led not only to strong interest in the physics of this new class of superconductors, but intense interest in potential applications for these materials. With superconductivity now accessible with relatively inexpensive nitrogen refrigerators, speculation and investigation of a wide range of technologies began.

The many potential applications of high-temperature superconductors involve use in both bulk and thin film forms. Among the possible uses for bulk material are such things as wires for numerous applications including magnets. As this work focuses on the study of thin films, those interested in further discussion of the applications of bulk material are referred to Ref. [3].

The uses of thin films of high-temperature superconductors may be roughly subdivided into three categories. The first category involves the use of the unique physical properties of the new superconductors to create specialized electronic devices. This category includes devices based on the Josephson effect, such as the superconducting quantum interference device (SQUID) [4]. The second category of application incorporates the superconductor within devices based on other technologies. This includes using superconducting interconnects and ground planes in semiconductor-based chips.

The third category of potential uses of high-temperature superconductor thin films takes advantage of the superconductor's ability to carry very large current densities. Such applications include tape conductors for electric power transmission and magnet windings. It is this third category that provided the initial motivation for the majority of the work to be discussed here, though much of the information contained herein may be useful in the development of uses belonging to all three kinds of application.

To produce a device such as a tape conductor, one must first consider the choice of appropriate substrate material. The single crystal materials

normally chosen for the controlled epitaxy of a crystalline material such as $YBa_2Cu_3O_{7-\delta}$ high-temperature superconductor are inappropriate for this kind of technology due to their inflexibility, cost, and limitations in size and shape. An ideal substrate material could be made into long tapes and/or wound into coils, requiring flexibility and the ability to fabricate in such forms. The material must also be compatible with the corrosive processing environment required for superconductor deposition. One such class of materials is the "stainless" polycrystalline metal alloys, including stainless steels and Ni-based "superalloys." However, as will be discussed later in this work, superconductor growth directly on these materials is limited by both chemical incompatibility and the fact that the substrate does not provide the proper crystalline structure needed in the growing superconductor film.

This work studies the development of an intermediate layer to solve this problem and enable the growth of $YBa_2Cu_3O_{7-\delta}$ thin films on substrates with which it is not normally compatible. In particular, the pulsed-laser deposition technique is investigated as a means of growing an intermediate layer of yttria-stabilized zirconia that is chemically compatible and provides the

proper crystalline template for superconductor growth. A unique aspect of this work is the employment of ion bombardment in conjunction with the pulsed-laser deposition process in order to control the orientation of a thin film. We are among the first to study this ion-assisted pulsed-laser depostion approach.

Though most of the work contained herein discusses deposition on a polycrystalline Ni-based superalloy, the intermediate layer technology developed here may be appropriate for many situations demanding the growth of a high-temperature superconductor thin film on a non-single-crystal substrate material. In fact, we believe that our results may be relevant to the deposition of thin films for many other applications, not just high-temperature superconductors.

2. $YBa_2Cu_3O_{7-\delta}$ THIN FILMS

2.1. $YBa_2Cu_3O_{7-\delta}$ Properties

In order to begin the discussion of $YBa_2Cu_3O_{7-\delta}$ (YBCO) thin films, it is necessary to first discuss some of the important properties of the material.

YBCO has a superconducting critical temperature T_C ~ 90-92 K and was the first material that displayed superconductivity above the boiling point of nitrogen [5]. Although other compounds with higher T_C's have been synthesized since, particularly the Bi-Sr-Ca-Cu-O (T_C ~ 110 K) [6], Tl-Ba-Cu-O (T_C ~ 125 K) [7], and Hg-Ba-Ca-Cu-O (T_C ~ 133 K) [8] materials, YBCO has remained the main focus of thin film research due to the demonstrated ease of growth of high quality films. Indeed, within months of the initial report of YBCO synthesis, promising thin films were deposited with the pulsed-laser deposition technique [9].

The high-temperature superconductors are Type II, or hard, superconductors. Type II superconductors are generally more useful for applications than Type I superconductors due to their ability to carry higher currents and remain superconducting in larger magnetic fields [10]. This is because Type I superconductors are superconducting up to a an applied magnetic field, known as the critical field (H_{c1}), at which point the entire superconducting sample becomes normal. On the other hand, Type II superconductors have two critical magnetic fields, H_{c1} and H_{c2}, the lower and upper critical fields. A Type II material excludes an applied magnetic field up to H_{c1}, but

allows gradually increasing flux penetration between H_{c1} and H_{c2} while remaining in the superconducting state. The penetrating flux is quantized in units of $\phi = \pi hc/e$, known as fluxoids [11]. Though the material at the center of flux lines is not superconducting, the rest of the sample remains superconducting up to H_{c2}. This allows the Type II superconductors to withstand higher magnetic fields than Type I superconductors, as well as pass higher currents, since current flow generates magnetic fields.

YBCO is a member of the so-called "double-layered 1-2-3" class of high-temperature superconductors of the formula $RBa_2Cu_3O_{7-\delta}$ (R = Y, Eu, Dy, etc.) [12]. The crystal structure of YBCO, shown in Fig. 2.1, is an oxygen deficient perovskite structure. The features of this structure are symmetric about the center Y layer. The layer on either side of the Y layer is the Cu-O_2 plane layer, in which each copper is coordinated by four oxygen atoms in the *a-b* plane. This plane layer is common to all of the high-temperature cuprate superconductors, and is thought to be the location of the superconducting current [13]. Surrounding the Cu-O_2 plane layers are the Ba-O layers, which contain one O for each Ba. Finally, between the Ba-O layers is the Cu-O chain layer.

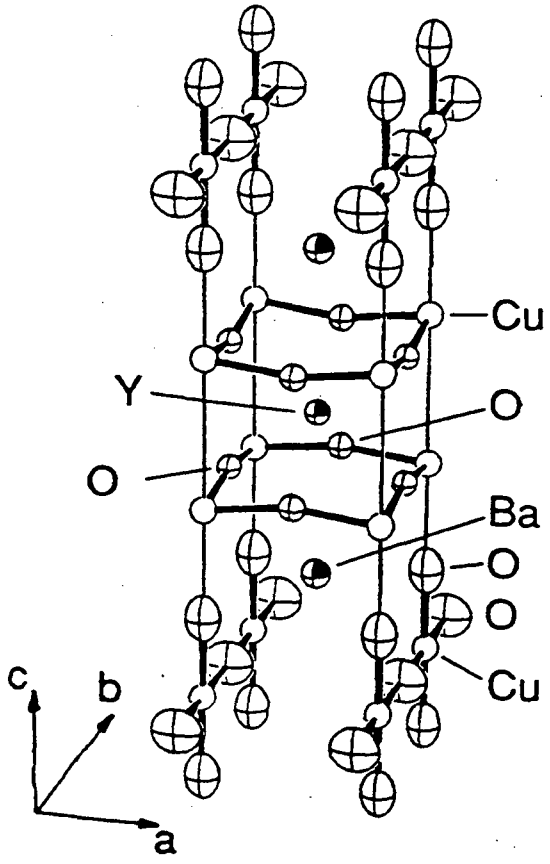

Figure 2.1. Orthorhombic structure of $YBa_2Cu_3O_7$. (Reproduced from Ref. [12].)

When YBCO is fully oxygenated (δ=0), half of the oxygen sites in this layer are unoccupied and the oxygen atoms order along the *b* axis, forming Cu-O chains. It is this layer that is affected when YBCO is not fully oxygenated. As oxygen is lost from this layer, the ordering of the Cu-O chains decreases, until ordering is lost at $\delta \sim 0.6$ [14]. This represents a change in structure from orthorhombic when the chains are ordered and $a \neq b$, to tetragonal when ordering is lost and $a = b$.

The T_C of YBCO is highest for $0 \leq \delta \leq 0.1$, corresponding to its orthorhombic phase with lattice parameters of $a \sim 3.82$, $b \sim 3.89$, and $c \sim 11.68$ Å [15]. T_C drops with increasing δ and the material is no longer superconducting upon transition to the tetragonal phase when $\delta \geq 0.6$ [14]. Therefore, control of stoichiometry and phase purity is critical for YBCO synthesis.

As can be seen in Fig. 2.1, YBCO has a very anisotropic structure. This leads to strong variations in the measured superconducting properties with orientation. Ginzburg-Landau coherence lengths have been estimated to be $\xi \sim 5$-7 Å parallel to the *c*-axis and $\xi \sim 20$-30 Å perpendicular to the *c*-axis [16]. Thus, it can be said that the directions of preferred superconductivity lie parallel to the Cu-O, or *a*-*b*

planes. Indeed, superconducting critical currents (J_C's) have been found to be an order of magnitude greater in directions perpendicular to the *c*-axis than in the *c*-axis direction. For this reason, YBCO films for current-carrying applications must be grown in the *c*-axis-normal orientation; i.e., grown with the *a-b* planes in the direction of current flow parallel to the substrate surface.

Another aspect of YBCO that must be considered in thin film development is the effects of grain boundaries on the superconducting behavior of polycrystalline films. It has been shown that grain boundaries exhibit a so-called "weak link" behavior that is highly dependent on the boundary angle between grains. Dimos *et al.* [17] investigated this phenomenon by growing a series of pairs of small crystals, or "bi-crystals," with controlled grain boundary angles and found that the superconducting current flow between the grains scaled approximately linearly with the inverse of the boundary angle. Ivanov *et al.* [18] performed similar work, but added a higher-temperature anneal step than in the Dimos work, and showed a nearly exponential dependence of J_C with inverse boundary angle. This weak-link behavior has been found in numerous thin film experiments, including the ground-breaking work of Norton *et al.* [19], who

compared the J_C's of YBCO films on single crystal and randomly-oriented polycrystalline yttria-stabilized zirconia (YSZ) substrates. Though c-axis films were grown on both substrates, it was shown that a film on the polycrystalline substrate carried nearly two orders of magnitude less current than a film on the single crystal substrate. This was due to the fact that there was no alignment of the *a-b* in-plane axes on the randomly-oriented polycrystalline substrate, leading to the presence of high-angle grain boundaries in the film.

As is the case when depositing thin films of any material, the chemical and thermal compatibility of YBCO with substrate materials must be considered. The chemical compatibility of YBCO is particularly difficult to manage. The diffusion of trace amounts of many different elements into YBCO has been demonstrated to adversely affect or destroy superconductivity [20-22]. Also, at the high temperatures necessary for YBCO growth (up to 800 °C), YBCO reacts with many substances [23]. Next, the necessity of the high growth temperatures raises issues of thermal compatibility. Since YBCO films will be grown at high temperatures and then cooled to below T_C for use, it is apparent that the thermal expansion properties (YBCO room temperature coefficient of linear expansion $\alpha \sim 13.6$ μm/m°C) of

a substrate material must be reasonably similar to those of YBCO to avoid cracking and other problems. Thus, the chemical and thermal properties strongly limit the range of materials that can be used with YBCO.

2.2. Epitaxial Films

2.2.1. Growth on Compatible Substrates

The first growth of a superconducting YBCO thin film was reported by Dijkkamp *et al.* at Bellcore [9] using the pulsed-laser deposition technique. In their study, both $SrTiO_3$ and Al_2O_3 single crystal substrates were used but it was determined that Al_2O_3 was not suitable for direct deposition of YBCO due to chemical reaction at the interface. $SrTiO_3$, on the other hand, proved suitable, and has since gained wide acceptance as a preferred substrate for YBCO thin film process development. Besides its chemical compatibility, $SrTiO_3$ has thermal expansion characteristics similar to YBCO and has a perovskite structure with lattice constant of a = 3.905 Å, providing a reasonable lattice match for c-axis YBCO growth (within ~ 2%). High quality YBCO films on $SrTiO_3$ substrates typically have T_c's > 90 K and J_c's higher than 5×10^6 A/cm^2 at 77 K have been reported [24-26].

The growth is highly epitaxial in nature, as evidenced by x-ray diffraction measurements showing precise alignment of crystal axes and YBCO (005) rocking curve widths $\Delta\omega < 0.65°$ [27], and by transmission electron microscopy proving atomic registry [28].

Several other single crystal substrates have been demonstrated to provide epitaxial YBCO growth with a high degree of compatibility. These include yttria-stabilized zirconia (YSZ), $LaAlO_3$, MgO, $LiNbO_3$, and other similar materials [29-33]. In all of these cases, the growth of epitaxial YBCO films with little or no interface reaction (a thin region of intermediate composition of less than 100 Å has been found in some instances) has produced superconducting layers with T_C's > 90 K and J_C's > 10^6 A/cm^2.

2.2.2. Growth on Incompatible Substrates Using Intermediate Layers

There are many substrate materials that are technologically significant but that are incompatible with YBCO due to chemical interactions between the film and substrate, such as interdiffusion and the formation of unwanted phases. Among the most important are the common semiconductor materials; Si and GaAs, and sapphire.

For YBCO deposition on Si, early investigations [34-36] showed Si diffusion into the film and Cu diffusion into the substrate, along with a region of enriched Ba and oxygen content near the interface. C. T. Cheung and E. Ruckenstein [23] later established the formation of Ba_2SiO_4 in this region by x-ray diffraction. They also showed that under some conditions, CuO and 211-phase (Y_2BaCuO_5) are formed. Similar results were demonstrated for sapphire, with strong Al diffusion into the YBCO and the formation of $BaAl_2O_4$, CuO, and 211-phase.

Many attempts have been made to deposit YBCO films directly on Si and SiO_2 substrates (for a review see Ref. [37]). In all cases, the films have been shown to have poor crystalline quality due to the reactions at the film-substrate interface. This has led to depressed T_c's ($\leq$ 85 K) and poor J_c's, the best reported being only about 10^4 A/cm^2 at 4.2 K [38].

To solve this problem, several researchers have grown intermediate layers of materials such as YSZ [39-42] and MgO [43,44]. These layers grow epitaxially on the single crystal substrates and in turn provide for subsequent epitaxial YBCO growth, reducing or eliminating the problem of chemical interaction. J_c's as high as 2×10^7 A/cm^2 at 4.2 K and 2.2×10^6 A/cm^2 at 77 K have been reported for

deposition on Si with a YSZ intermediate layer [40].

2.3. Non-Epitaxial Films/Use of Intermediate Layers

In order to expand the range of YBCO thin film applications, the deposition of YBCO films on substrates on which epitaxial growth is not possible, or in some cases, not wanted, is desirable. Proper epitaxial growth is not possible on amorphous substrates or substrates that do not have an appropriate lattice match with YBCO. In some cases, such as in the use of randomly-oriented polycrystalline substrates, some degree of epitaxy may be possible but is not desirable. This is due to the properties of YBCO discussed in Section 2.1 that necessitate development of *c*-axis films with alignment of the in-plane axes. If a YBCO film was to grow epitaxially on a randomly-oriented polycrystalline substrate, the YBCO would then itself be polycrystalline and contain detrimental high-angle grain boundaries.

The use of a randomly-oriented polycrystalline Ni-based superalloy substrate material for a YBCO thin film tape conductor application is an example of a non-epitaxial case. Even if some degree of

epitaxy occurred during growth on this substrate, it would not be desirable as it would not produce a c-axis film with in-plane alignment. As will be shown in Section 7.2, YBCO deposition on such a substrate results in a thin film of poor crystalline quality. In addition, it will be shown that YBCO is chemically incompatible with this type of substrate. Clearly, an approach to eliminate direct contact of the YBCO and the substrate is needed.

The use of an intermediate layer of compatible material, as in the case of epitaxial YBCO films on chemically incompatible substrates discussed in Section 2.2.2, is a possible solution. However, a major obstacle still remains: it is still necessary to control the structure and orientation of the YBCO film without an epitaxial template from the substrate. Thus, an intermediate layer is needed that has an appropriate crystalline structure and can be grown in the proper orientation for subsequent YBCO growth. In other words, the approach taken here is to develop an intermediate layer that will provide for proper epitaxial growth of a c-axis YBCO film on itself even though this layer did not grow epitaxially on the substrate. This investigation explores processing methods to

control the orientation of yttria-stabilized zirconia intermediate layers.

3. YTTRIA-STABILIZED ZIRCONIA (YSZ) THIN FILMS

3.1. YSZ Properties

Zirconia, ZrO_2, is a widely studied ceramic material [45,46] that has been used for many applications. In particular, cubic-phase yttria-stabilized zirconia (YSZ) is interesting due to its stability over a wide temperature range, oxygen-ion conductivity, and chemical inertness [45]. YSZ thin films have been used in a wide range of applications, from solid electrolytes in gas sensors and fuel cells [47], to insulating layers in microelectronic devices [48]. Deposition of thin films has been demonstrated by a variety of techniques, including sputtering [49], electron beam evaporation [50], and pulsed laser deposition [36]. The chemical formula of YSZ is $(Y_2O_3)_x(ZrO_2)_{1-x}$.

Pure zirconia has a monoclinic structure at temperatures up to 1170 °C, while from 1170 to 2370 °C, its structure is tetragonal [45]. Above 2370 °C, up to the melting point of 2680 °C, it is cubic.

The cubic phase has the fluorite-type structure, with each zirconium atom surrounded by eight equidistant oxygen atoms, and each oxygen surrounded by four zirconiums. This structure is shown in Fig. 3.1. When ZrO_2 is alloyed with one of many di- or trivalent oxides that have cubic symmetry, such as CaO, MgO, and Y_2O_3, the phase transition temperatures are lowered. In several cases, if an appropriate amount of alloying oxide is added, the cubic-fluorite structure can be stabilized down to room temperature. This occurs with the addition of Y_2O_3, as indicated in the binary phase diagram shown in Fig. 3.2 [51]. Though the exact minimum amount of Y_2O_3 necessary to stabilize the cubic phase is still the subject of some controversy, it is now generally agreed that adding about $x > 0.05$ provides stabilization, up to the solubility limit near $x \sim 0.3$ [46]. Over this range of composition, the lattice constant varies from $a \sim 5.13$ Å to $a \sim 5.18$ Å.

Because the oxides that stabilize cubic zirconia are di- and trivalent, while the zirconium cation is Zr^{4+}, a defect structure must exist to maintain charge balance within the crystal. In 1943, Wagner [52] determined that CaO-stabilized zirconia contained a large number of oxygen

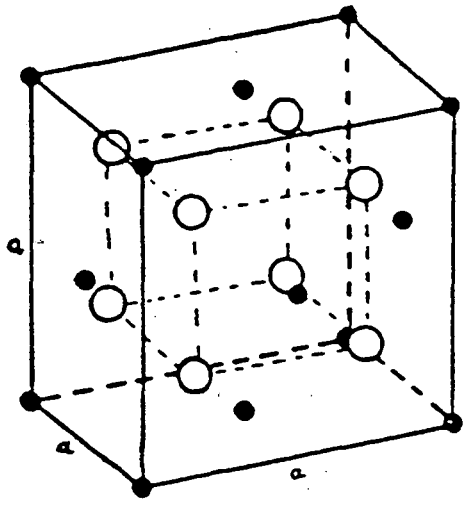

Figure 3.1. Fluorite-type structure of cubic ZrO_2. (Reproduced from Ref. [45].)

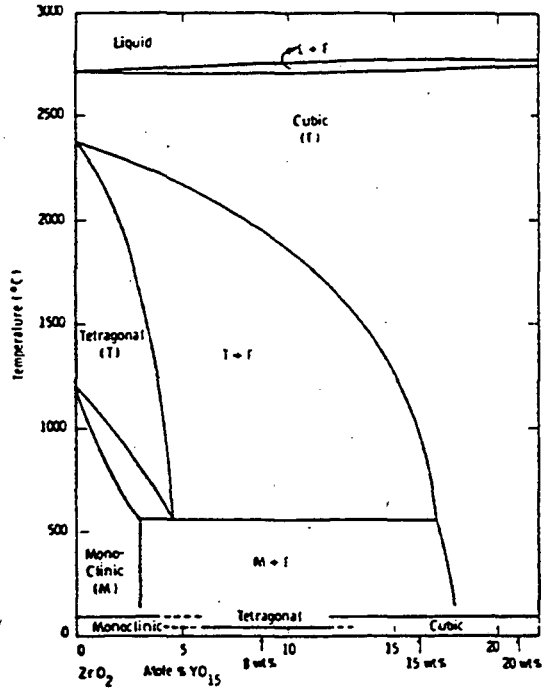

Figure 3.2. Binary phase diagram for the Y_2O_3-ZrO_2 system. (Reproduced from Ref. [45].)

vacancies. Following this work, Hund [53] showed that Ca^{2+} and Zr^{4+} are statistically distributed over the cation sites, and that the charge neutrality is maintained by the creation of oxygen vacancies equal in number to the Ca^{2+} concentration. This defect structure has since been established for all of the stabilized zirconias. For YSZ, the addition of trivalent Y_2O_3 leads to the formation of one oxygen vacancy for every two Y^{3+} ions.

The oxygen vacancy defect structure of YSZ is responsible for several of its useful properties. First, the high concentration of oxygen vacancies and resultant ease of oxygen diffusion gives YSZ its oxygen conductivity and makes it useful for applications such as oxygen sensors. Second, the anion vacancy structure and charge neutrality considerations lead to a very low cation vacancy concentration, even at elevated temperatures. Since most cations are too large to diffuse through the interstitial sites in zirconia and will not diffuse on the oppositely charged vacancy sites, one observes very low cation diffusion rates [54]. Indeed, cation diffusion coefficients in YSZ have been shown to be a millionfold smaller than oxygen diffusion coefficients [55]. This makes YSZ an

effective barrier against the diffusion of most metallic elements. Also, this factor contributes to the stability of YSZ, as transtions from the cubic phase require cation diffusion [45].

The mechanism by which the cubic phase of zirconia is stabilized by alloying is not well understood. Though Y_2O_3 is itself cubic, it is surprising that the addition of only ~ 5% Y_2O_3 to zirconia causes such a dramatic lowering of the temperature at which the normally very-high temperature cubic phase is stable. However, studies of undoped ZrO_2 have shown that when the oxygen content is reduced below normal stoichiometry to produce anion vacancies, the cubic phase stability region of the phase diagram becomes larger [56]. Thus, the stability of the cubic phase seems to be related to oxygen vacancies.

A H. Heuer and M. Ruehle [57] have proposed that the stability of the cubic phase arises from a change of the electronic energy contribution to the free energy caused by the defect structure. They point to the quantum mechanical calculations of M. Morinaga *et al.* [58], which compare the electronic structure of the cubic and tetragonal phases of pure ZrO_2. According to these calculations, the tetragonal phase has a higher degree of covalency,

which leads to a larger band gap and a lower valence band energy. Therefore, they predict that the tetragonal phase is stable at lower temperatures due to the electronic energy contribution to the overall free energy. The stability of the cubic phase at T > 2370 °C is attributed to the increased contribution of the higher entropy of this higher symmetry phase. In stabilized or oxygen deficient zirconia, local structural relaxation occurs around the anion vacancies, and atoms are slightly displaced from their ideal cubic-fluorite positions. The calculations predict that this changes the electronic structure significantly, moving it closer to the tetragonal phase. Therefore, they propose that the entropy contribution to the free energy predominates in stabilized zirconia, leading to the preference of the cubic phase at lower temperatures.

3.2. Use as Intermediate Layer for YBCO Thin Film Growth

Single crystal substrates of (001) YSZ have been successfully demonstrated as suitable substrate materials for YBCO thin films [59,60]. The room temperature coefficient of thermal

expansion of YSZ is $\alpha \sim 11.6$ μm/m°C, reasonably similar to that of YBCO ($\alpha \sim 13.6$). *c*-axis YBCO epitaxy with a lattice mismatch of < 0.2% has been demonstrated for the in-plane epitaxial relationship YBCO[100]//YSZ[100] [61], with four unit cells of YBCO for every three of YSZ [62].

As mentioned in Section 2.2.2, several researchers have studied the use of YSZ as an intermediate layer for YBCO epitaxial growth on Si and other substrates that are not compatible with direct YBCO deposition. D. K. Fork *et al.* [63] have demonstrated epitaxial growth of (001) YSZ on (001) Si, with the in-plane epitaxial relationship YSZ[110]//Si[110]. Resultant YSZ films had (002) rocking curve widths of $\Delta\omega \sim 0.7$-$0.8°$, indicating the presence of little tilt in the film. This value is good for a film grown on a dissimilar substrate material. (See Section 6.3.1.2 for a discussion of rocking curves.) Subsequent growth of a YBCO film produced a high quality film with YBCO (005) $\Delta\omega \sim 0.6$-$1.0°$ [40], close to that obtained for YBCO on $SrTiO_3$ single crystals [27]. Resultant $T_C > 90$ K and $J_C \sim 2.2 \times 10^6$ A/cm^2 at 77 K, demonstrate the feasibility of the use of YSZ intermediate layers for YBCO thin film growth.

4. PULSED LASER DEPOSITION OVERVIEW

Though the idea of depositing thin films of material using an intense laser beam first arose in 1965 [64], the use of pulsed-laser deposition (PLD) has only recently become popular. This is partly due to the fact that the necessary high energy laser technology has only become prevalent in the past few years. However, perhaps the main reason that the use of PLD has boomed recently is that the technique was the first used to successfully deposit a superconducting YBCO thin film in 1987 [9]. It took a few years before proponents of more common deposition techniques such as sputtering were able to grow YBCO films that were similar in quality to those being grown by PLD. Because of this, and the subsequent realization by many researchers that PLD is a fairly easy-to-use technique, the use of PLD has exploded to the point that the deposition of films of at least 128 different materials have been documented in recent years [65].

4.1. Pulsed-Laser Deposition Concept

The concept and experimental use of PLD is quite simple. The radiation from a high energy

pulsed laser, most commonly an excimer laser, is focused onto a target of the material to be deposited within a vacuum chamber. The substrate upon which the thin film is to be grown is set directly across from the target. Under the appropriate conditions, material will be removed from the target by each laser pulse and form a plume of vapor expanding outward along the normal to the target surface. Some of the ejected material collects on the substrate to form the film. Though seemingly simple, the actual physical process of material removal is very complex and is currently the subject of intense research [66-68].

In the simplest approach one can consider the laser material removal mechanism to be a two-step process: first, the laser energy is absorbed, and then, material is expelled or vaporized. The "first step" begins with the absorption of the laser radiation energy, generating energetic electrons and phonons in the material. At the high energy densities (> 1 J/cm^2) and short pulse widths used for PLD (or power densities > 10^7 W/cm^2), rapid heating occurs in the surface and near-surface region. For most materials of interest, especially metals and small-bandgap materials, the optical absorption depth is shorter than the thermal diffusion distance [69]. Thus, the rate of

heating near the surface is rapid compared to the rate of thermal dissipation, and melting and vaporization occur.

Continuing with this simple description, the "second step" of the laser-material interaction is the ejection of material due to the recoil pressure created by the vaporization process. This process has been modeled as an expulsion caused by a mechanical shock wave originating below the target surface due to rapid expansion from local superheating [70]. This type of approach explains observations that the plume of ejected material is very forward-directed, with empirical measurements showing distributions near $(\cos\theta)^{10}$, where θ is the angle of deviation from the target normal [67]. This is far different from the $\cos\theta$ dependence normally observed for pure thermal evaporation. Also, whereas thermal evaporation produces a vapor composition dependent on the vapor pressures of each element in the material, this laser-induced material expulsion produces a plume with stoichiometry similar to the target.

Of course, this two-step description of the laser ablation mechanism is an extreme simplification of a very complex process. One of the most important components not considered in this description is the creation of a plasma above

the target surface and the subsequent interaction of the laser radiation with the plasma. The plasma is initiated by thermal emission of electrons and ions from the target. This plasma expands rapidly as the electrons, ions, and ejected atoms and molecules interact and continue to absorb laser radiation. Models indicate that once the plasma is formed (in the first few nanoseconds), the plasma itself may absorb some of the remainder of the laser pulse by inverse bremsstrahlung scattering [67]. This absorption is highly dependent upon many other factors, including the laser wavelength, pulse intensity, plasma density, and plasma temperature. At the relatively high pressures (10^{-3}-10^{-1} Torr) and pulse intensities typically used for PLD of materials like YBCO, the plasma is likely to absorb part of the laser radiation [71].

The net result of the laser-target interaction is the production of a highly energetic plume of material travelling away from the target surface. Mass and emission spectroscopies have shown that a plume can contain many species, including electrons, neutral atoms and molecules, and charged ions [69]. In the case of YBCO ablation in oxygen, the presence of neutral and charged Y, Ba, and Cu has been shown, along with mono- and di-oxides such as CuO, YO, and BaO_2. It is interesting to note

that when YBCO was ablated in vacuum, CuO was not observed, indicating that a gas-phase reaction occurs in the presence of oxygen [72]. Ion probe measurements of YBCO ablation in vacuum indicate that the fraction of ionized material in the plume is < 10% [73]. Time-of-flight experiments have found expansion velocities for neutrals of 10^5 to 10^6 cm/s and as high as 10^7 cm/s for charged species in vacuum. This corresponds to kinetic energies of roughly 1 to 10's of eV for most material and as much as 100 eV for ions. It is important to note, however, that in the pressure regime usually employed to deposit films such as YBCO, the mean free path is about 1 to 10 mm, so collisions are likely to reduce these energies significantly before arrival at the substrate surface.

4.2. Advantages for Thin Film Growth

The characteristics of the laser ablation process produce several advantages for thin film growth. First, the fact that the material ejected from the target has a composition similar to the target provides for congruent material transfer to the substrate for film growth. This is particularly advantageous in the depostion of films

with complex stoichiometry, such as YBCO. Only in a few cases has it been demonstrated that it is not possible to grow a film with the same composition as the target by PLD, and in these cases, such as the loss of Pb content in the deposition of Pb-doped Bi-Sr-Ca-Cu-O films [74], the problem is likely caused by the high vapor pressure of one component leading to its evaporation from the growing film. This difficulty exists no matter which deposition technique is chosen.

Another advantage of PLD lies in the energetics of the process. It has generally been found in thin film growth research using energetic deposition techniques that atoms arriving with energies of 1 to 10 eV promote film densification and have a high sticking probability [75]. This is precisely the range of energy expected at the substrate in PLD, and can be controlled to a certain degree by simply changing the target-substrate spacing. Moving the substrate closer to the target puts it into the more energetic part of the plume, whereas moving it away lowers the energy of the plume material through collisional processes. This energy can also be changed easily by variations in pressure (higher pressure reduces mean free path) or laser energy density.

Yet another advantage of PLD is the ability to conduct the process in high partial pressures of reactive gas, such as oxygen. This is crucial for the deposition of YBCO in order to maintain the proper oxygen content in the film. Also, the presence of a reactive gas can help bind volatile species to a substrate, maintaining stoichiometry.

Finally, there are several instrumental advantages to the use of PLD in comparison with other common deposition techniques. For example, the vacuum requirements for PLD are not as demanding as for some other techniques, such as molecular beam epitaxy (MBE). PLD requires a base pressure of only about 10^{-5} to 10^{-6} Torr, whereas lower than 10^{-8} Torr is usually required for MBE [76]. A distinct advantage over sputtering is that PLD does not require maintenance of a constant glow discharge, which can limit process parameter control and lead to preferential resputtering of a growing film by charged ions. Also, in contrast to sputtering, PLD does not require specialized targets - one simply places a piece of the material to be deposited on a holder. Lastly, some of the above advantages combine to make it quite easy to deposit multiple film layers of different materials *in situ*.

5. ION-ASSISTED THIN FILM GROWTH

The bombardment of a thin film with ions during deposition has been found in many cases to produce changes in film properties. The term *ion-assisted deposition* (IAD) is generally used to refer to processes in which film properties are purposely modified by controlled ion bombardment during growth.

Ion bombardment is an inherent component of the process in many sputtering and plasma deposition processes; ions of the appropriate charge generated in a plasma are attracted to the electrode on which the substrate sits. Often, the substrate will be purposely biased to attract or repel ions, or to change their energy. When the process utilizes this ion bombardment to affect film properties, it is appropriately called IAD. One of the difficulties involved in these types of IAD processes, however, is that the electrode biases, input power, and pressure are not independent variables, leading to a limited degree of control over ion energies and flux.

An increasingly more common method to achieve controlled ion bombardment during film growth is to use a separate ion source, such as a Kaufman source

[77,78]. A Kaufman source allows independent control of ion bombardment direction, energy, and flux. (In plasma processes, plasma parameters sometimes limit the degree to which this independence can be achieved.) Thus, precise control of IAD-modifiable thin film properties can often be achieved.

It is important to note that in this work, ion-assisted pulsed-laser deposition (IAPLD) is the focus of my studies. As PLD is a relatively new process technique, very little information exists in the literature on the use of an ion beam in conjunction with PLD. One important consideration is the fact that PLD is a pulsed rather than a continuous process, resulting in a non-continuous arrival of material to the film growth surface. As a Kaufman source provides a continuous ion bombardment, there was some question as to whether IAPLD would yield film modifications similar to those obtained with other IAD techniques. Nearly all existing information on the use of IAD involves the use of processes that provide continuous arrival of material to the film surface, such as sputtering and evaporation techniques.

5.1. Modification of Film Properties

A comprehensive list of film properties that can be modified by IAD would be very long. Since ions of sufficient energy striking a film physically displace atoms, film microstructure is directly affected. Thus, any property that is directly or indirectly related to the microstructure may be changed by IAD. Also, ions striking the surface impart energy to the atoms at and near the surface, thereby influencing kinetic processes during growth. Many researchers have used this aspect of IAD to reduce film growth temperatures, as properties normally expected at higher temperatures can be obtained at lower temperatures since the ion bombardment provides the necessary energy to the growth region [79]. Reducing growth temperatures has advantages in many thin film deposition processes, particularly in reducing chemical interactions and diffusion between substrates and films.

One of the most common uses of IAD is to provide the densification of films during growth. This is particularly important in the area of optical coatings, where porosity can lead to difficulty with stability and reproducibility of the refractive index. This porosity arises from

the fact that many films grow in the Volmer-Weber or island growth mode, especially at low temperatures [80]. When adatom mobility is low, arriving atoms tend to stick where they land, leading to irregularly-shaped islands. Also, the island tops see a greater flux of incoming material than the lower areas, causing so-called shadowing effects. As the islands coalesce, voids are created. Bombardment with an ion beam can enhance adatom mobility, leading to increased packing density. IAD can be said to help change a Volmer-Weber growth process toward a more layer-by-layer, or Frank-van der Merwe mode. This effect has been demonstrated in the deposition of many different materials, including Ag [81], SiO_2 [82], Ge [83], CaF_2 [84], and ZrO_2 [85].

Of particular relevance to this study is the work of P. J. Martin *et al.* on the modification of properties of ZrO_2 optical films using an ion-assisted electron-beam evaporation process [86]. By adding a 600 V Ar^+-beam to their evaporation process, the film packing density was increased from 0.83 to nearly 1.0. A corresponding increase of the refractive index from 1.84 to 2.23 was found. More surprising, however, was the observation of a change in the predominant ZrO_2 phase in the film. Without ion-assistance, the

films were shown to contain mostly the monoclinic phase, as is expected for pure ZrO_2 from the equilibrium phase diagram (see Fig. 3.1). On the other hand, IAD-grown films were found to consist predominantly of cubic phase material. Thus, the introduction of ion-assistance changed an equilibrium-like growth process to a non-equilibrium process producing a metastable phase.

Other film properties that are frequently modified using IAD include film stress, adhesion, grain size, step coverage, and crystalline orientation [79]. As the control of orientation of non-epitaxial YSZ intermediate layers for YBCO thin film growth on randomly-oriented polycrystalline substrates is the goal of this work, a review of previous studies of IAD effects on film orientation follows.

5.2. Control of Thin Film Orientation

5.2.1. Previous Studies

Although the effects of ion bombardment on film orientation during thin film growth were first noted as long ago as 1977 [87], very few comprehensive studies of this potentially powerful IAD technique have appeared in the literature. What exists are several diverse studies and

observations of IAD effects on a wide range of film materials.

In 1977, Marinov [87] reported that using an Ar^+-beam of several kV during Ag film growth changed the preferred orientation from (111) to (110). At that time, Marinov made little mention of the potential applications of such a method nor did he attempt to provide a detailed theoretical explanation for the observed effect. It was not until 1982 that Dobrev [88], noting the same effects for IAD of both Ag and Au, pointed out that the change in orientation seemed to be related to the direction of the incoming ions. Dobrev observed that the preferred orientation under ion bombardment was one in which the ion direction corresponded to a crystal channeling direction. He offered a further theoretical explanation for this that will be discussed in the next section.

Following the work of Marinov and Dobrev, several other researchers reported similar relationships between IAD film orientation and beam direction along a channeling axis in other metals, such as Cu [89], Al [90], and Ni [91], and other materials including Si [92] and AlN [93]. However, most of these studies looked only at ion beams directed at normal incidence to the substrate, and none checked for orientational effects in the

azimuthal, or in-plane, directions. For the present case of depositing a YSZ intermediate layer for YBCO superconductor growth, we know from the discussion of YBCO properties in Section 2.1 that it is necessary to align the in-plane axes as well as the c-axis-normal orientation to eliminate the weak-link effects of high-angle grain boundaries. Therefore, it is desirable to know if IAD can be used to control in-plane orientation.

In 1985, L. S. Yu *et al.* [5] published an investigation of the effects of using glancing-angle ion bombardment during IAD sputtering of Nb films, looking for the first time for possible effects on in-plane axial alignment. Without ion-assistance during deposition, the Nb films were found to display a high degree of (110)-normal texture, but random alignment of the grains in-plane. The addition of a 200 V Ar^+-beam at 20° from glancing angle produced two significant effects. First, the film was found to have near-(110)-normal alignment but the grains were tilted 5 ° toward the beam direction. This corresponded to an orientation in which the ions see a planar channeling direction between (110) planes. Second, an x-ray pole figure revealed a preferred alignment of the in-plane axes. Yu speculated that this was caused by a preferred sputtering mechanism and this

theory was further developed by the same collaborators in a subsequent article by R. M. Bradley *et al.* [94] that will be described in the next section.

Since the publications of Yu and Bradley several more reports have appeared on the orientational effects of IAD for various materials and a few brief summaries of such findings have been published in reviews of IAD techniques [79,95]. However, little further work studying the effects of such aspects as ion-beam parameters on the degree of azimuthal orientational control has appeared, nor has any detailed investigation of the potential applications of this technology.

5.2.2. Theory

As mentioned above, Dobrev [88] was the first to propose that the IAD orientational control was related to the channeling directions of ions in the crystal. He further hypothesized that this was due to the fact that the density of energy deposition would be inversely related to the depth of channeling. According to the "thermal spike" calculations of F. Seitz [96], a one kilovolt bombarding particle may cause a local increase in temperature of 10^4 K for a time interval of about 10^{-11} s over a region containing 10^3-10^4 atoms.

Thus, in a polycrystalline film, the grains that had their channeling directions aligned to the beam would be effectively "cooler" than other grains, and would thereby act as nucleation centers for recrystallization of surrounding material heated by the "thermal spike." By this mechanism, Dobrev proposed that the film would become dominated by this recrystallization process under continuous bombardment during growth thereby producing a film with the predominant orientation aligned to the ion beam.

On the other hand, Bradley *et al.* [94] proposed that the dominant mechanism that caused IAD orientational alignment was a preferential sputtering process. They pointed to the studies of others that showed strong dependency of sputter rates on angle of ion incidence for single crystal diamond [97] and copper [98]. The lowest sputtering rates were shown to be for orientations that had a crystal channeling direction parallel to the angle of ion incidence. Thus, grains of material that were not aligned would have their growth impeded relative to the aligned grains due to this higher sputtering rate by the ion beam. Eventually the aligned orientations would predominate. Bradley then constructed a detailed model with parameters for differences in sputter

yields, degree of natural self-epitaxy, and the ratio of ion flux to deposition vapor flux. The results of calculations with this model showed good qualitative agreement with the results of Yu *et al.* [5] for Nb deposition.

These two theories actually are quite similar in that both assume that the orientational effects are due to the difference in the energy transfer process caused by the alignment or misalignment of channeling axes to the energetic ion beam. The main difference is a question of viewpoint - Dobrev prefers to consider it a process of growth of the aligned crystallites by a recrystallization process that takes material away from the other grains, while Bradley looks at it as a process of shrinkage of the misaligned relative to the aligned crystallites due to preferential sputter removal of material.

6. EXPERIMENTAL

6.1. Pulsed-Laser Deposition

6.1.1. System Overview

A pulsed-laser deposition (PLD) system was designed and built specifically for this research

project. A Questek model #2860 excimer laser using KrF gas to emit 248 nm wavelength radiation was chosen. According to the manufacturer's specifications, this laser produces 20-30 ns pulses of up to 750 mJ energy at a repetition rates of 1-5 Hz. In practice, it was found that energies of up to only 500-600 mJ/pulse could be obtained reliably and reproducibly. Using a quartz lens to focus the rectangularly-shaped beam to a spot size of about 2x4 mm at the target translates to a maximum possible energy density of approximately 7.5 J/cm^2. However, as the laser beam in this setup is first reflected toward the vacuum deposition chamber by a mirror, then passes through the quartz lens, and finally passes into the chamber through a quartz window, a measurement of the actual energy near the target site was made. This measurement indicated that for a 600 mJ pulse at the laser, the actual energy density is about 4 J/cm^2 at the target.

A diagram of the deposition vacuum chamber is shown in Fig. 6.1. The chamber is pumped by a Balzers model #TCP310 turbomolecular pumping system rated to pump up to 500 liters/s. All permanently mounted devices, such as thermocouple and power feedthroughs, were sealed using Conflat-type copper gasket ultra-high vacuum seals, while the quick-access door and rotary push/pulls use rubber o-

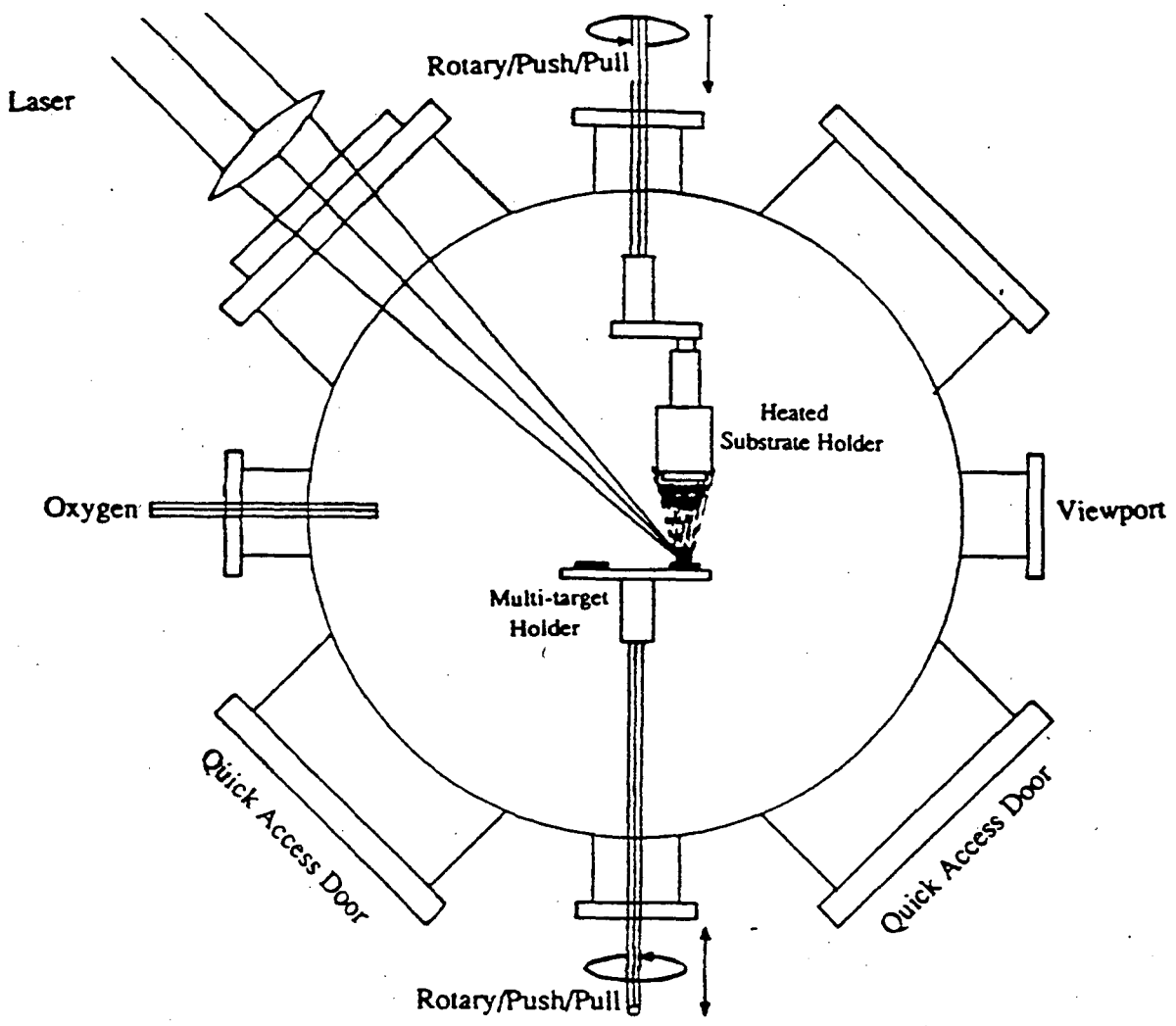

Figure 6.1. Top view of the pulsed-laser deposition vacuum chamber. Not shown is the ion source, which is mounted below the rotary push/pull feedthrough.

rings. This enables a system base pressure of ~ 10^{-7} Torr following continuous overnight pumping. For deposition runs, a base pressure less than 10^{-5} Torr is routinely obtained in less than one hour before commencing a process run.

A substrate heater was devised using a coiled Kanthol wire resistive element in a ceramic block. A cover plate of Haynes Alloy #230 was made. To reduce radiative heat loss, a thin foil of stainless steel was wrapped around most of the heater block, except the area of the cover plate where substrates are mounted. This enables temperatures of up to 800 °C to be obtained in oxygen atmospheres up to several hundred mTorr. The temperature was measured using K-type thermocouple wires attached to the cover plate just below the substrate with a small screw. Temperature is controlled using an Omega model #CN2042 temperature controller. It is important to note that all temperatures reported here are measurements at the face of the cover plate, which should represent the temperature on the backside of the substrate.

To provide gas atmospheres for deposition and ion-source gases for ion-assisted processes, a gas flow control system was devised. First, a Varian variable leak valve was installed to deliver oxygen

over a wide range of flow rates for both deposition atmospheres and chamber venting. No direct measurement of flow rate is obtained with this device. For precise delivery of low flows (1-1000 sccm), a Vacuum General model #UV2-21 mass flow controller was installed. A system of valves allows the introduction of either oxygen or any other available gas, most frequently argon, through this controller. This system is directly connected to the ion gun to provide ion-source gas when the gun is in use or normal gas flow when the gun is off. A Vacuum General model #CMO capacitance manometer measures process pressure, which is controlled using a combination of a gate valve between the chamber and the turbopump, and an adjustable iris flow constrictor.

The Kaufman-source ion gun, a Commonwealth Scientific 3 cm tungsten-filament ion source, is mounted below the target holder and the push/pull feedthrough and is thus not shown in Fig. 6.1. The gun was mounted on a stand that could be moved back and forth to allow some variation of source-substrate spacing, but unfortunately had to be physically bent to allow changes in ion-beam angular direction! (A new stand to allow precise angular adjustment is under development.) The gun was configured with a single Ni-mesh grid, allowing

a beam voltage range of approximately 50 to 200 volts. Beam currents from about 5 to 60 milliamps could be obtained. As previously mentioned, a mass flow control system provides precise control of source gas flows of oxygen, argon, or any other gas that is installed.

6.1.2. Typical Deposition Conditions and Procedures

Prior to every deposition run, the substrate is rinsed in deionized water followed by methanol, and then attached to the substrate heater with silver paint. Following evacuation of the chamber to < 10^{-5} Torr, a preheat cycle is performed for any deposition that will be run below 500 °C. The heater is ramped to 500 °C (taking approximately 10 minutes), held at this temperature for 10 minutes, and then allowed to cool to the desired deposition temperature. This cycle drives any remaining solvent from the silver paint and volatilizes contaminants on the substrate surface. Tests of longer preheat cycles did not produce any further pressure drop, indicating that this cycle effectively removes any contaminants that can be driven off.

For depositions below 500 °C in a gas atmosphere, gas flow is started and the pressure

set when the temperature reaches the deposition temperature. For runs at higher temperatures, gas is introduced during the temperature ramp-up when the temperature reaches 500 °C. A typical deposition temperature for YBCO growth is near 750 °C, while temperatures from room temperature to 700 °C have been used for YSZ depositions. To provide full stoichiometric oxygen composition in most oxide films, including YBCO and YSZ, deposition is carried out in an oxygen atmosphere. A typical oxygen pressure for YBCO growth is 200-300 mTorr, while for YSZ it is less than 100 mTorr. Once the deposition temperature and pressure are stabilized, the target surface is precleaned using a few laser pulses while a shutter blocks the substrate.

It has been shown that congruent material removal from YBCO and similar oxide materials usually occurs for laser energy density above a threshold of approximately 1 J/cm^2 [69]. Thus, depositions are typically performed at a laser energy of 400-500 mJ/pulse, giving an energy density at the target of 2-3 J/cm^2. This provides assurance that the congruence threshold is safely exceeded, while running at an energy that the Questek excimer laser can routinely achieve. A pulse repetition rate of 5 Hz is most often used. It has been found that varying the pulse rate from

1 to 10 Hz does not change the film properties, so once again this parameter was chosen by safely using an energy level that the laser could routinely produce. Using these parameters, a typical YBCO deposition rate is about 1 angstrom/pulse, or 300 angstroms/min.

Following all depositions at elevated temperatures, the deposition chamber was filled to near atmospheric pressure with oxygen through the Varian valve prior to turning off the heater. The heater was then shut off, and the sample allowed to cool to room temperature. This procedure essentially provides a short oxygen anneal during the cooldown cycle. It has been shown to be important for proper oxygenation of YBCO films, which transform from the tetragonal to the superconducting orthorhombic phase near 400 °C in an oxygen atmosphere greater than ~ 1 Torr [99].

Additional deposition parameters and procedures for ion-assisted depositions will be discussed in Section 7.3.3.

6.2. Materials Specification and Preparation

6.2.1. Substrates

6.2.1.1. Haynes Alloy #230

Haynes Alloy #230 (HA230) is a Ni-based "superalloy" that is appropriate for tape conductor applications, as discussed in Section 1. It was chosen for this study due to its resistance to oxidation in high-temperature environments and chemical and structural stability to well over 1000 °C. Also, HA230 has a thermal expansion coefficient, α_{HA230} ~ 14-15 μm/m°C [100], that is similar to that of YBCO, α_{YBCO} ~ 13-14 μm/m°C. The elemental composition of HA230 is shown in Table 6.1. HA230 is polycrystalline with no preferred grain orientation. The ASTM grain size is 4-5, indicating predominant grain sizes of 50-200 μm. The crystal structure is the same as that of pure Ni, FCC, with some slight variation in lattice parameter due to the substitution of other elements in the FCC lattice. The carbon content of HA230 produces both intra- and inter-grain carbide particles which enhance chemical and structural stability by providing resistance to grain growth at elevated temperatures, as well as providing high mechanical strength.

Element	Cr	W	Mo	Fe	Co	Mn	Si	Al	C	La	B	Ni
%	20.0-24.0	13.0-15.0	1.0-3.0	3 max.	5 max.	0.3-1.0	0.25-0.75	0.20-0.50	0.05-0.15	0.005-0.05	0.015 max.	balance

Table 6.1. Haynes Alloy #230 elemental composition.

Circular substrates of HA230 are first cut from 0.6 mm sheet. As HA230 arrives from the manufacturer with what is known as a "pickled" surface which is very rough, the substrates must be polished. The circular substrates are mounted in a resin block mold for surface polishing. The pickled surface is first removed using a rough lapping paper, and then polished using aluminum oxide powders on a mechanical lapping wheel. The grit size of the finishing polish is 0.05 μm. It is usual among metallurgists to assume a finished surface roughness no greater than half the grit size of the final polish. A scan using a Dektak Profilometer revealed surface features no greater than 10 nm. The substrates are removed from the resin by dissolving the resin in acetone. They are then rinsed further in acetone and deionized water, and stored awaiting deposition.

6.2.1.2. Other substrates

All other substrates used in this work were used as obtained from the manufacturer. Polished 0.5mm-thick (100) $SrTiO_3$ single-crystal substrates for YBCO process definition (see Section 5.7.1) were obtained from Atomergic Chemical, Inc. Polished 1.0mm-thick fused-silica substrates were also purchased from this vendor. The polycrystalline alumina and Teflon materials used for the quick tests described in Section 7.3.3 were secured from random stock of unknown origin in the Lawrence Berkeley Laboratory machine shops. Both were approximately 0.5 mm thick. These substrates were not polished or treated in any way, other than the usual cleaning in deionized water and methanol.

6.2.2. Targets

YBCO targets for thin film deposition were made by James Wu at Lawrence Berkeley Laboratory. Starting materials of 99.99% or better purity were used and careful measuring procedures insured Y:Ba:Cu ratios of 1.00:2.00:3.00. Target disks of 1/2 to 3/4 inch diameter and 2 to 3 mm thickness were provided. A resistivity versus temperature measurement showed these targets to be superconducting at > 90 K.

Excess material from the production of YSZ sputtering targets was purchased from Puretech, Inc. for YSZ deposition. Specifications for these targets indicate a guaranteed purity of 99.99% and a Y_2O_3 content of 10 molar-% for cubic-phase stabilization. Sections of about 1 inch square and 1/4 inch thickness were obtained.

6.3. Characterization Techniques

6.3.1. X-ray Diffraction

6.3.1.1. 2θ diffraction

2θ X-ray Diffraction (XRD) is performed on a Siemens Model 5000 Diffractometer. The thin film is placed in the diffractometer with the plane of the substrate normal to the diffractometer axis, as shown in Fig. 6.2(a). In this configuration, diffraction only from crystal planes parallel to the substrate surface is measured. In this way, the normal-axis orientation of a film can be determined. For example, for the YBCO film in the desired c-axis-normal orientation, only the (00*L*) series of peaks should be observed. The presence of any other peak indictates material of different orientation.

XRD can be used to determine or infer many other properties of a material, including the

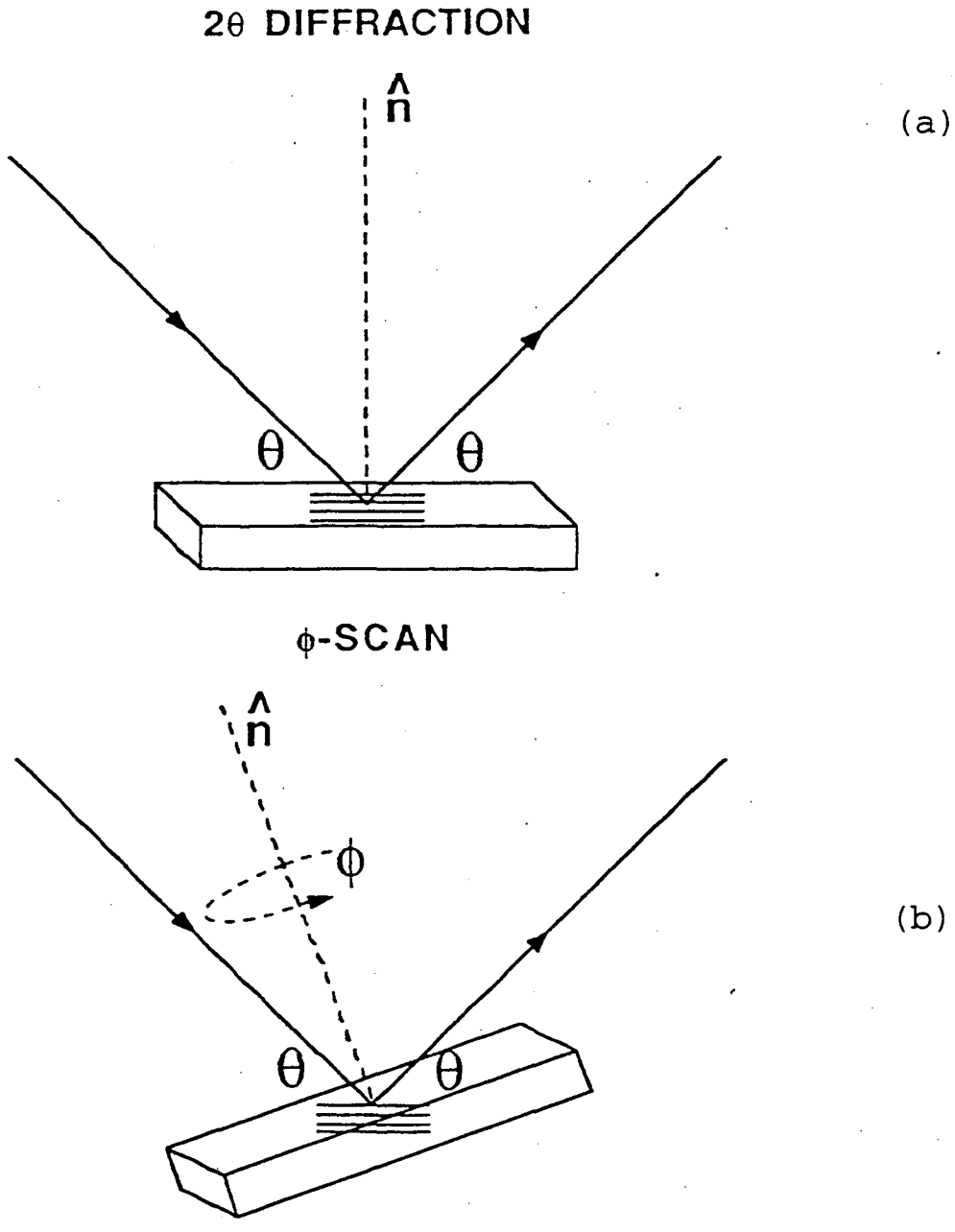

Figure 6.2. Configurations for x-ray diffraction measurements: (a) standard 2θ diffraction, and (b) ϕ-scans.

lattice parameter, phases present, and grain size [101]. The lattice parameter is calculated from the position of diffraction peaks using the relationship that governs x-ray diffraction, Bragg's Law, $\lambda = 2d\sin\theta$, where λ is fixed by the x-ray source. The presence of specific phases can be verified by the existence of peaks corresponding to the lattice structure of that phase. Finally, small grain sizes can be inferred from the broadening of diffraction peaks that occurs for grain sizes below approximately 10 μm [101]. This broadening is described by the well-known Scherrer formula, $t = (0.9\lambda)/(B\cos\theta)$, where t is the grain diameter, λ is the x-ray wavelength, B is the peak broadening (in radians), and θ is the Bragg diffraction angle.

6.3.1.2. ϕ-scans and rocking curves

X-ray ϕ-scans and rocking curve measurements were performed at Conductus, Inc. through collaboration with S. Garrison. A Siemens Four-Circle Diffractometer was employed for this purpose.

X-ray ϕ-scans can be used to determine the orientation of crystal axes in the plane of a film. The configuration for this measurement is displayed in Fig. 6.2(b). As shown in the figure, the thin

film sample is tilted in order to cause diffraction from planes not parallel to the substrate surface. It is then rotated about the film-normal to measure the presence of diffraction from these planes as a function of rotation. The tilt angle is set to an angle corresponding to the angle of a particular set of planes in the film. For example, the angle is set to 54.7 degrees for a (001) YSZ film to measure diffraction from the (111) planes, because the (111) planes form this angle with the film normal. Continuing with this example, if the in-plane axes in this film are well-aligned, four peaks of (111) intensity should be seen in a 360 degree rotation, as determined by crystal symmetry. However, if the film grains are randomly-aligned in the plane of the film, the ϕ-scan will be featureless.

Rocking curve widths were determined using the same confuguration as shown in Fig. 6.2(a). The sample is placed at a θ value corresponding to a Bragg diffraction peak, and then rocked about θ while the x-ray source and detector are held fixed. This width of the resultant curve is a direct measure of the range of orientation present in the film, because each slightly tilted region in the film will successively come into the diffracting position as the crystal is rotated [101]. Typical

rocking curve widths are 0.01 to 0.1 degrees for high quality single crystals, but higher values expected for polycrystalline materials and for thin films grown on dissimilar substrates.

6.3.2. Electrical Measurements

6.3.2.1. Resistance versus temperature

The resistance of YBCO thin films as a function of the temperature can be measured using a computer-controlled helium-cooled cryostat system developed by P. Berdahl and coworkers at the Lawrence Berkeley Laboratory [102]. The resistance is determined employing a standard four-probe technique [76]. Four thin (50-100 μm diameter) gold lead wires are attached to the film in a straight line using a Dupont silver conducting paint. AC current is passed through the outer two wires and the voltage drop is measured by the inner two wires. An EG&G Princeton Applied Research Lock-In Amplifier Model #5301 is used to provide both the current source and the voltage measurement. A Keithley Model #195A Digital Multimeter measures the current in the circuit. An IBM PC is programmed to record the temperature, current, and voltage, and calculate the resistance at intervals of 4 K or when resistance changes by more than 20% as the sample is cooled from room

temperature. Further description of this system can be found in Ref. [102].

A plot of the resistance versus temperature for a YBCO film contains a great deal of information. One not only receives direct measurement of electrical behavior, but one can also make inferences about the structural characteristics from this data. Properties that are measured directly include the superconducting critical temperature, T_C, the superconducting transition width, ΔT_C, and the slope of the normal-state resistance. T_C is the temperature at which the film no longer has a measurable resistance, and can be compared to the known values for bulk YBCO (T_C ~ 92 K).

ΔT_C is the difference between the temperature at which the onset of superconductivity is observed and the temperature at which resistance reaches zero (T_C). This is commonly defined by the temperatures at which the resistance is 90% of the pre-transition value to the 10% value. For pure superconducting-phase YBCO material ΔT_C is < 1 K [24]. A wider transition can be an indication of non-uniformity in the material. If the transition is wide, this indicates that a complete superconducting path is not available to provide zero resistance until a lower temperature than that

at which superconductivity is first observed. Thus, some regions in such a film may have lower T_C than others; i.e., non-uniformity may exist. A wide transition can also be caused by poor conduction between grains. The onset may be observed when the intra-grain resistance reaches zero, while there is still an inter-grain resistivity that limits the current path until a lower temperature.

The slope of the normal state resistance as a function of temperature can serve as an indicator of the phase purity in a YBCO thin film. Superconducting orthorhombic phase YBCO that is fully oxygenated exhibits metal-like conduction in the normal state, with a linear resistance slope pointed toward zero at zero temperature. It has been shown that this slope decreases with decreasing oxygen content in orthorhombic YBCO, with a change in the sign of the slope indicating a switch from metal-like to semiconductor-like behavior occuring at severe oxygen deficiencies approaching the transition from orthorhombic to tetragonal phase [14]. This effect has also been shown for YBCO that is doped by contaminants.

6.3.2.1. Critical Current Density

In order to make measurements of critical current densities (J_C), a patterning technique was devised using the excimer laser. A 50 μm wide bridge approximately 1 mm in length is created by taping a gold wire onto the film in the configuration shown in Fig. 6.3. The tape and the wire serve as a mask, while the unmasked material is removed by ablating with ~ 1 J/cm^2 laser pulses. About 20 to 30 pulses completely removes the unmasked YBCO. The tape is carefully removed and the four-probe contacts are made as above. The criterion used to define the critical current is the current at which the voltage across the bridge is 1 μV. The use of this criterion is accepted practice in the superconductivity literature. The J_C measurements are made in the same cryostat setup as the resistance measurements, though control and recording of the parameters must be performed manually. Also, a 0.4 T magnet is available to enable determination of J_C's in magnetic field.

6.3.3. Other Techniques

Auger depth profiling was used to investigate the elemental composition as a function of depth in deposited films. In particular, the technique was employed to determine the abruptness of the

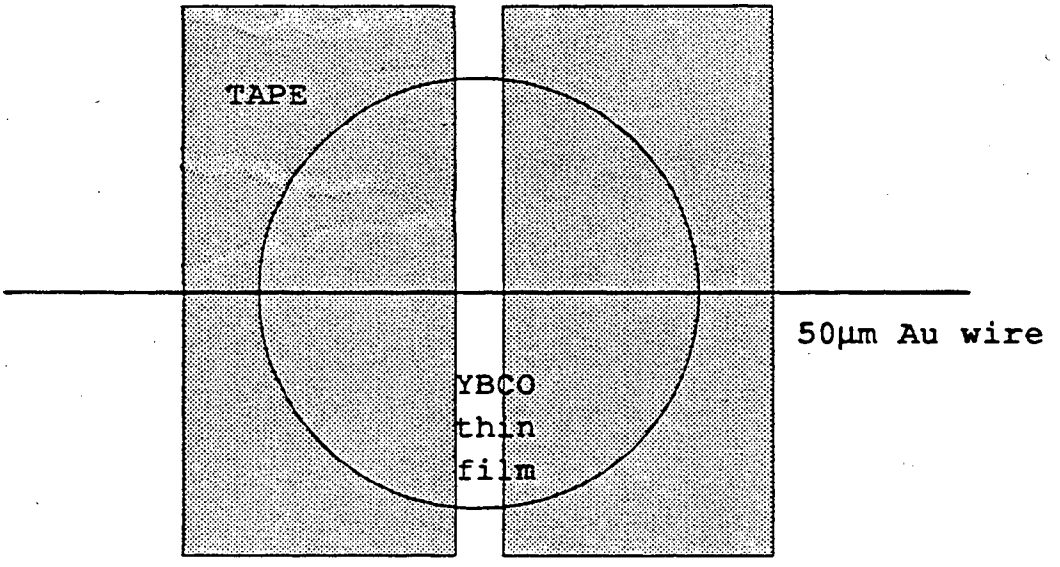

Figure 6.3. Mask used to pattern 50μm x 1mm YBCO bridge for critical current density measurements.

interfaces between layers and whether or not diffusion of elements occurred across these interfaces. To obtain a depth profile, the sample is alternately sputtered and then irradiated by electrons to produce characteristic Auger-electron emission by elements. This cycling is continued for many times until the desired depth is reached, and then an elemental depth profile is assembled from the Auger emission intensities measured for each cycle. The depth resolution of an Auger profile can be estimated as approximately 5% of the sputter depth, due to surface roughening caused by the sputtering process.

Film thicknesses reported in this work were measured using a Dektak Profilometer. A step corresponding to the film thickness was created on test samples by masking an area on the substrate during deposition. The mask was then removed and the thickness determined by measuring the step with the profilometer.

7. RESULTS

7.1. $YBa_2Cu_3O_{7-\delta}$ Deposition on $SrTiO_3$ for Process Definition

As has been discussed, the main subject of this research is the study of the growth of an appropriate intermediate layer for YBCO thin film growth on substrates on which epitaxial growth is not possible. However, as the ultimate test of such an intermediate layer is to measure the superconducting properties of a YBCO layer grown upon it, it was first necessary to develop a YBCO deposition process capable of producing "state-of-the-art" films. For this purpose, a PLD process to grow YBCO films on $SrTiO_3$ single-crystal substrates was developed. (The use of $SrTiO_3$ as a substrate material for YBCO thin films was discussed in Section 2.2.1.)

7.1.1. Process Parameters

A series of 0.5-1.0 μm YBCO thin films was deposited using the procedures detailed in Section 6.1.2. The general range of parameters to investigate was clear from the collaborative studies of R. E. Russo and B. L. Olsen at Lawrence Livermore Laboratory that led up to this work and

from the results of the pioneering investigations of the Bellcore group led by T. Venkatesan that were just being revealed at the time this work began [9,36]. The process parameters listed in Table 7.1 have been found to produce films with superconducting properties similar to the best reported in the literature. Films grown using these conditions are smooth and shiny-black in appearance and exhibit a superconducting critical temperature T_C > 90 K. By far the most critical process parameter was determined to be the temperature. As the deposition temperature is lowered from the optimum of 760 °C, the resulting T_C drops rapidly until no superconductivity is observed in films deposited below approximately 600 °C. Above 760 °C, films become rough and gray and exhibit lower T_C.

Changing the deposition rate by varying the laser pulse rate between 1 and 10 Hz does not affect the superconducting properties. Oxygen pressures from 200-300 mTorr produce films with T_C > 90 K. Below about 100 mTorr, T_C drops rapidly and films change from shiny-black toward a dull brown, indicating an oxygen deficiency. Increasing the pressure above 300 mTorr causes the deposition rate to drop quickly; therefore, higher pressures were not considered. The target-substrate spacing

of 5-7 cm puts the substrate at the rose-colored tip of the laser-induced plume. Placing the substrate closer in the brighter and hotter blue/white part of the plasma results in rough gray-ish films. Larger spacing gives film quality similar to that at 5-7 cm, but the deposition rate drops with increased distance.

Process Parameter	Optimum Value
pulse energy density	2-3 J/cm^2
pulse rate	1-10 Hz
oxygen pressure	200-300 mTorr
heater temperature	760 °C
target-substrate spacing	5-7 cm
oxygen flow rate	200 sccm

Table 7.1. $YBa_2Cu_3O_{7-\delta}$ Pulsed-Laser Deposition Process Parameters

7.1.2. Film Characterization

A plot of the resistance versus temperature for a YBCO film deposited on $SrTiO_3$ with the process in Table 7.1 is shown in Fig. 7.1. The normal-phase portion of the curve is linear and the slope extrapolates closely to zero, indicating that the film is fully-oxygenated superconducting-phase

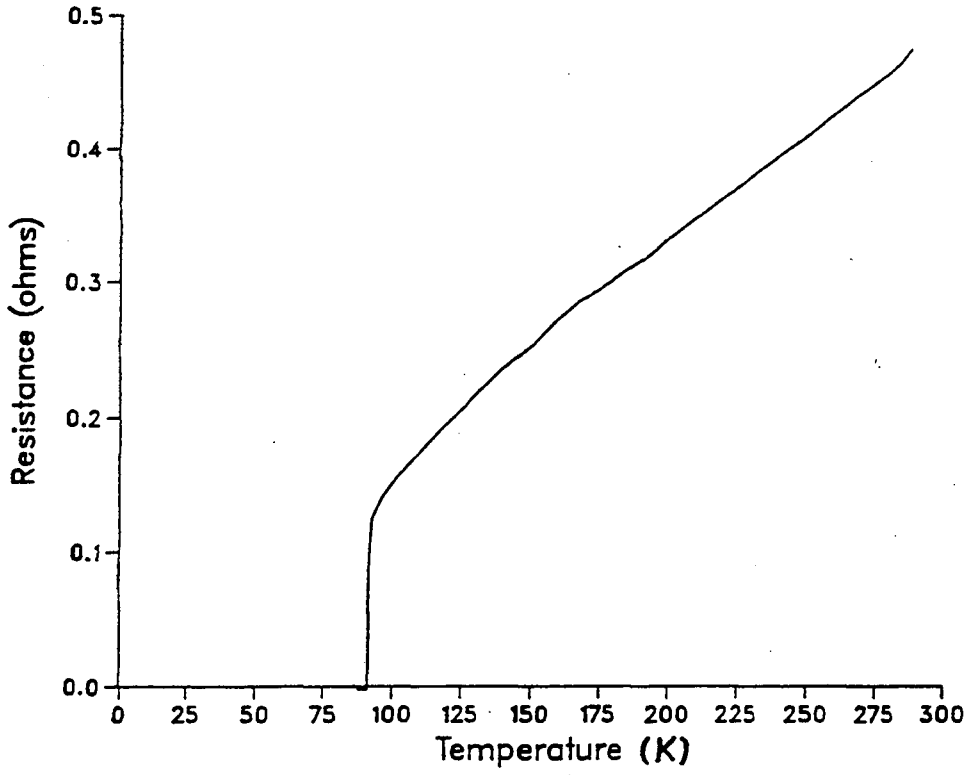

Figure 7.1. Resistance vs. temperature of a YBCO thin film grown on $SrTiO_3$.

(orthorhombic) material. The T_C of this film is 91.6 K. The superconducting transition width is $\Delta T_C < 1.0$ K, demonstrating further that the film is homogenous superconducting-phase material.

A rough measurement of the critical current density shows $J_C(77K) > 10^6$ A/cm^2. An exact measurement could not be made easily on this film due to problems with overheating of the lead wire contacts, which prevented any further increase in the current to the sample. However, as the highest reported values in the literature are near $J_C \sim 5\times10^6$ A/cm^2, this film clearly demonstrates superconducting properties similar to the "state-of-the-art."

A 2θ x-ray diffraction (XRD) scan for a film grown with this process is shown in Fig. 7.2. The presence of strong (00*L*)-series peaks proves the film to be highly *c*-axis oriented. There is no evidence of peaks for any other orientation. Also, a calculation of the c-axis lattice constant from the (00*L*) peak positions gives $c \sim 11.68$ Å, corresponding to the optimum orthorhombic-phase value.

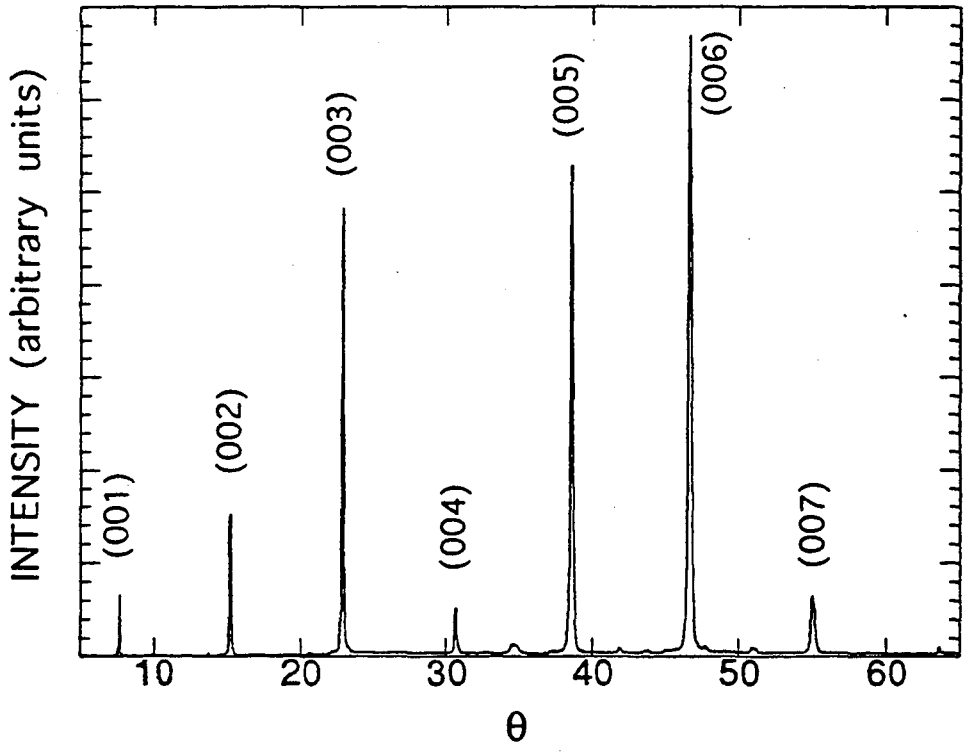

Figure 7.2. X-ray diffraction pattern of a YBCO thin film grown on $SrTiO_3$.

7.2. $YBa_2Cu_3O_{7-\delta}$ Deposition Directly on Haynes Alloy #230

Following the development of the YBCO PLD process using $SrTiO_3$ substrates, the growth of YBCO films directly on HA230 substrates was performed with this process. The highest T_C measured for such a film is less than 60 K. A resistance vs. temperature curve, shown in Fig. 7.3, demonstrates semiconductor-like behavior (negative slope) in the normal-state region, likely indicating contaminated or oxygen-deficient material. The wide $\Delta T_C > 30$ K shows that the film is not homogenous, with some regions superconducting at the onset $T_C \sim 90$ K but others providing resistance down to below 60 K. Deposition of films on other stainless steels and Ni-alloys yielded similar or worse results. Also, varying the process parameters, particularly the temperature, did not improve the film superconducting properties and in fact often worsened them.

An XRD scan on a YBCO film deposited directly on HA230 has YBCO peaks that are barely distinguishable from the background. Some c-axis texture is apparent but peaks of other orientations also appeared, indicating a largely randomly-oriented film. This is not unexpected, due to the

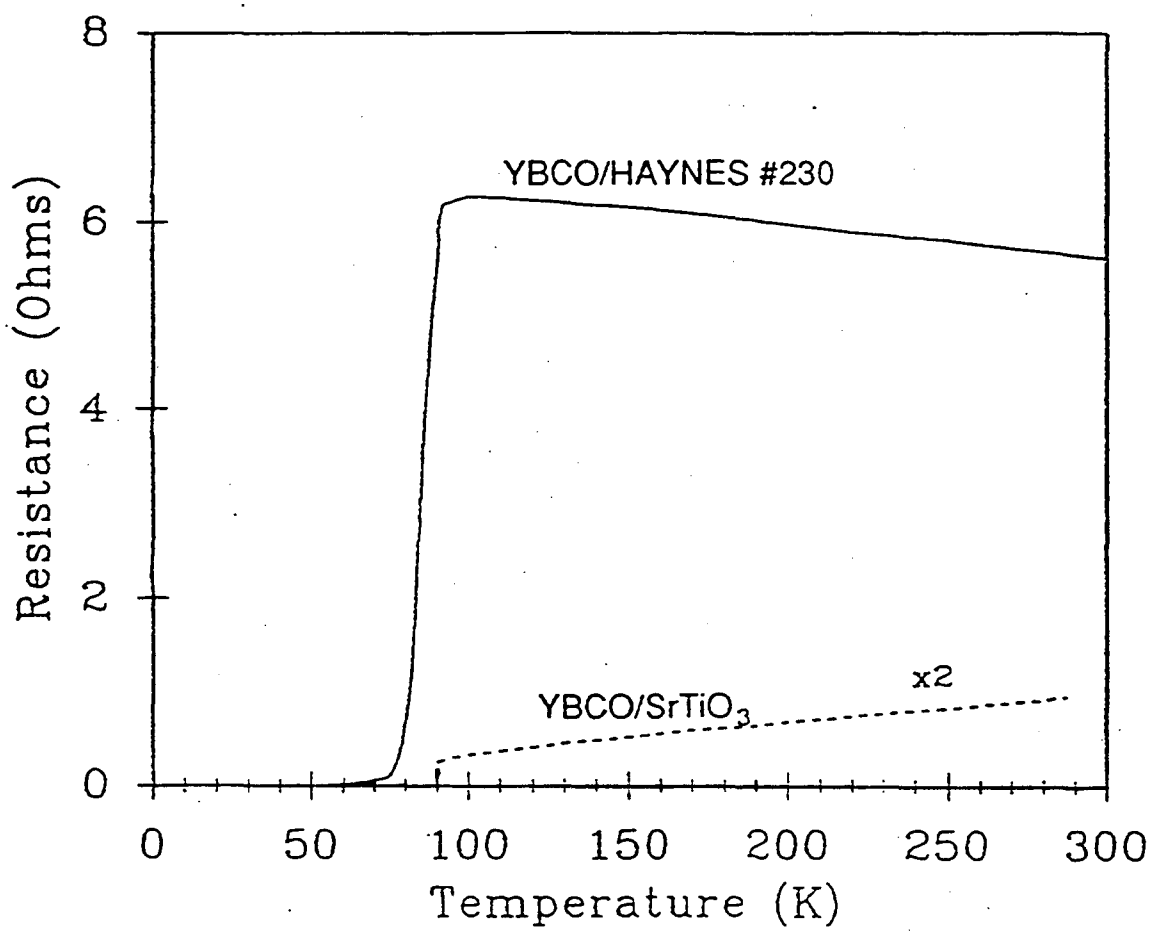

Figure 7.3. Resistance vs. temperature for a YBCO thin film grown directly on HA230. Data for a YBCO film on $SrTiO_3$ is shown for comparison.

fact that the substrate is a randomly-oriented polycrystalline material which does not provide the proper template for controlled YBCO c-axis growth.

The suspicion that the poor resistance vs. temperature characteristics shown in Fig. 7.3 are at least partially due to contamination of the YBCO film by diffusion of elements from the HA230 is confirmed by the Auger depth profile shown in Fig. 7.4. The depth resolution of this profile near the interface between the YBCO film and HA230 substrate is approximately 25 nm, yet the region in which both film and substrate elements are mixed extends over 0.2 μm. If the interface is defined to be at ~0.55 μm depth (where Ba, O, and Ni are all near half their average values), then Ni has diffused more than 0.1 μm into the YBCO, and Cr more than 0.05 μm. Also, there is clear distortion of the elemental ratios of the YBCO film from about 0.35 μm depth to the interface. The peak of Cu concentration at ~0.45 μm depth coincides with the lowest Ba concentration in the film and what appears to be a local maximum in the Ni content. At ~0.5 μm depth, the highest oxygen concentration is seen, along with a local peak in Ba and a Cu content of about 50% of the bulk film value. These features are probably due to reactions producing other compounds or phases, though none could be

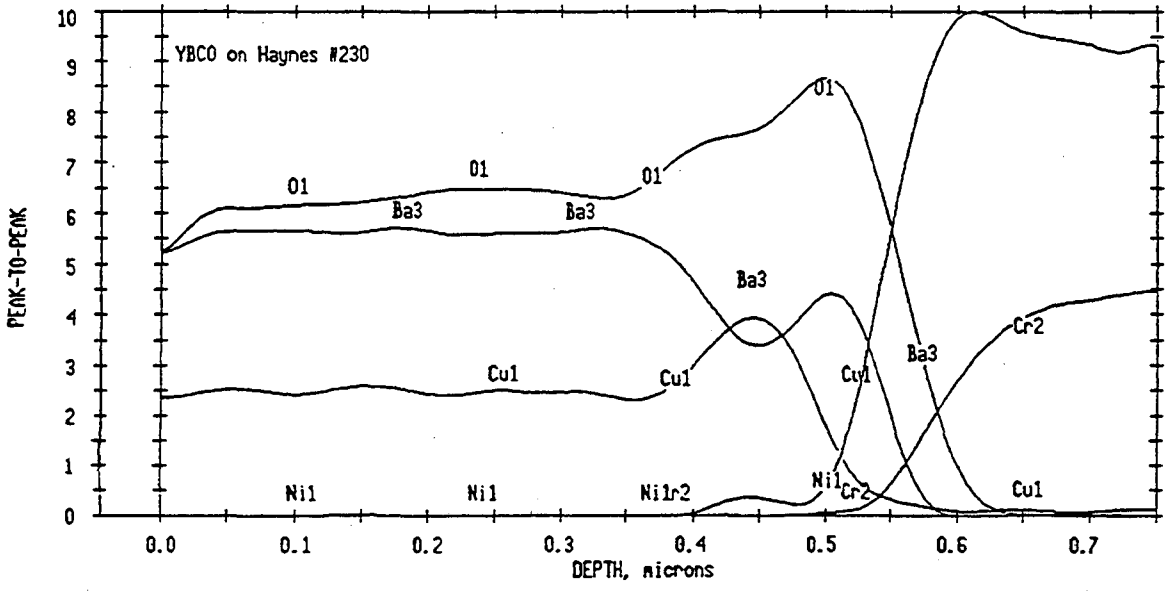

Figure 7.4. Auger elemental depth profile for a YBCO film deposited directly on HA230.

identified from x-ray diffraction. This is direct evidence of the chemical incompatibility of YBCO and HA230, and, along with the lack of the proper crystalline template for c-axis growth and the poor superconducting properties, clearly demonstrates the need for an intermediate layer. This layer must provide both a barrier to diffusion and the necessary crystal structure to seed *c*-axis YBCO growth.

7.3 Yttria-stabilized Zirconia Deposition on Haynes Alloy #230

7.3.1. Non-ion-assisted Deposition

Prior to the commencement of YSZ PLD on HA230 experiments it was noted that the then recent results of other groups, particularly D. K. Fork *et al.* [40], showed that PLD of (001) YSZ had been achieved for epitaxial growth on Si and other substrates. It was demonstrated that, as in the case of YBCO deposition, congruent material transfer occurred at laser pulse energy densities above approximately 1 J/cm^2, and that deposition in oxygen atmospheres gave pure cubic-phase material, as desired. Fork *et al.* [63] also investigated the effects of pressure and temperature on the YSZ orientation on (100) Si and reported that low

pressures and low temperatures resulted in primarily randomly-oriented or (111)-oriented YSZ, while higher pressures and temperatures provided the (001) orientation. The preference for (001) growth at higher temperatures is predictable, as this orientation has the closest lattice match to (100) Si, and elevated temperatures often enhance the epitaxial growth of the best-matched orientation due to the higher surface mobility during deposition. It is important to note, however, that in this case, the growth of YSZ is epitaxial on the single-crystal substrate. For YSZ on randomly-oriented polycrystalline HA230, the growth is not expected to be epitaxial, and is therefore likely to be affected differently by process pressure and temperature. Thus, a series of depositions was performed to investigate the effects of these parameters.

7.3.1.1. Temperature effects

PLD of YSZ was carried out at temperatures from 70 °C to 700 °C at different pressures. In all cases, the pulse energy density was approximately 2 J/cm^2 and the repetition rate was 5 Hz. The target-substrate spacing was kept between 4-5 cm. XRD patterns for films deposited at different temperatures in 1.0 mTorr of oxygen are displayed

in Fig. 7.5. The only diffraction peaks observed in these tests correspond to cubic-phase YSZ - no other crystalline phases are present. The film deposited at 70 °C shows a (002) diffraction peak, indicating (001) texture in the film. As the deposition temperature is increased, the (002) peak disappears and the (111) peak appears and increases in intensity. At 700 °C, strong (111) texture is evident. These trends are in direct contrast to the behavior discussed above for YSZ deposition on Si, indicating that in that case, the orientation at higher temperatures was dictated by the epitaxial relationship with the substrate. No such relationship exists in this case.

Although the desired (001) orientation is achieved at 70 °C, the (002) diffraction peak is broad and shallow. This indicates that although the film may show a preference for (001) texture, it is likely that the texturing is incomplete and the grain size is small [101]. Attempts were made to further the (001) texturing using post-deposition anneals, but only slight improvement was possible.

7.3.1.2. Pressure effects

XRD patterns for YSZ layers deposited on HA230 at pressures from vacuum to 100 mTorr of oxygen are

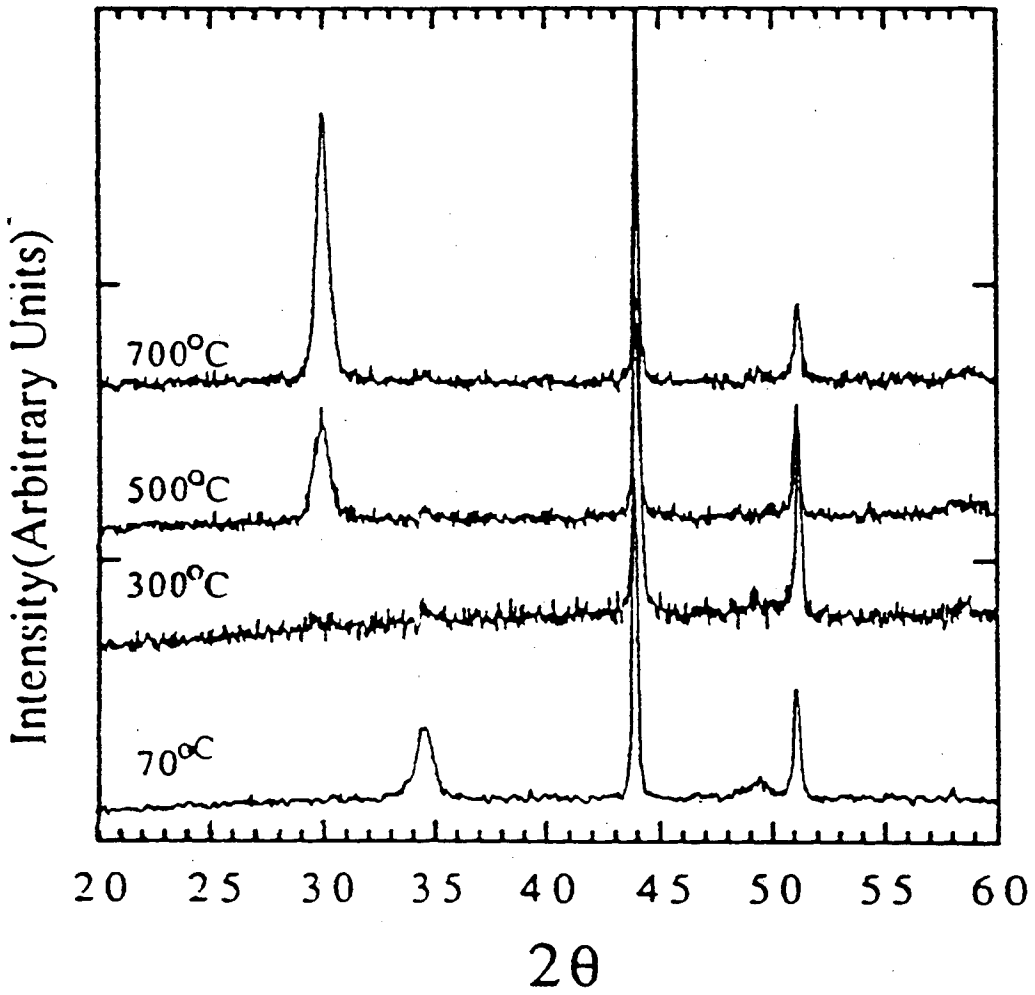

Figure 7.5. X-ray diffraction patterns for YSZ films deposited on HA230 at different substrate temperatures.

shown in Fig. 7.6. These films were grown at 50-70 °C, and the other process conditions were the same as above. Films deposited in oxygen pressures from 0.5 to 1.0 mTorr show a preference for (001) orientation, while those grown at higher pressures display some (011) or (111) texture. At 100 mTorr and above, as well as in vacuum, no crystalline texture is observed. Once again, these effects of pressure are different for those observed by others for epitaxial growth of YSZ on Si. The results of our pressure experiments, as well as the temperature experiments above, were repeated to confirm these trends. The (001) and (111) texturing at the conditions described reproduced consistently. For reasons that are not understood, the appearance of the (022) peak at intermediate conditions was inconsistent.

7.3.1.3. Suitability of layers for $YBa_2Cu_3O_{7-\delta}$ deposition

From the investigations of PLD process parameter effects on YSZ film orientation, it is clear that the (001) orientation desired for YBCO growth can be obtained at 1.0 mTorr oxygen pressure and 70 °C. However, as discussed above, the broad and shallow (002) XRD peak shows that these layers are not completely textured. Also, an x-ray ϕ-scan

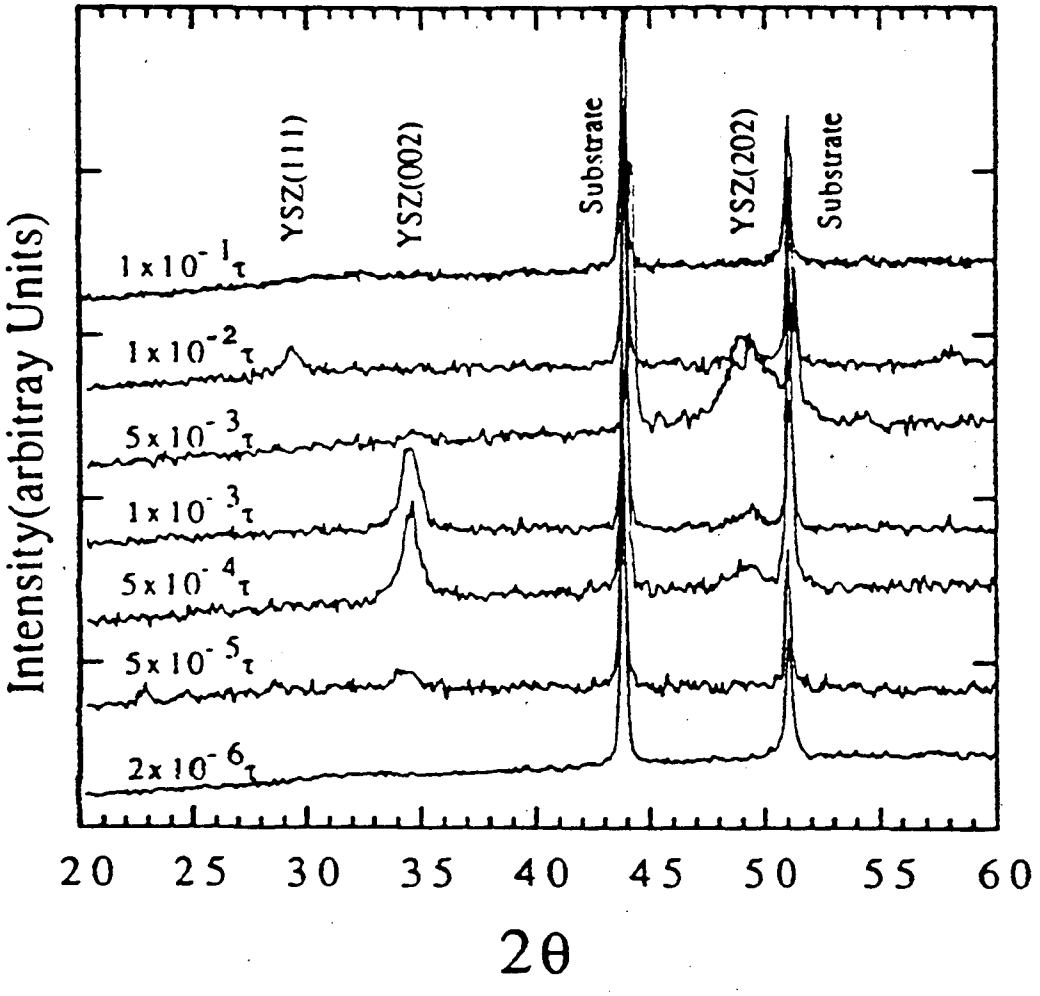

Figure 7.6. X-ray diffraction patterns for YSZ films deposited on HA230 at different oxygen pressures.

showed no preferred in-plane texture. Thus, the suitability of this type of layer for YBCO growth needed to be tested.

A YBCO thin film was deposited on the (001) YSZ intermediate layer on HA230 discussed above using the process defined in Table 7.1. An Auger elemental profile for this film is shown in Fig. 7.7. This profile is remarkably different than the one of Fig. 7.4 for a YBCO film deposited directly on HA230. In this case, there is no evidence of any diffusion between the YBCO and the YSZ or between the YSZ and the HA230, and the elemental ratios are consistent throughout each film. Also, the interfaces are abrupt to within the limits of the measurement. Clearly, the YSZ serves as a good diffusion barrier between YBCO and HA230.

An XRD pattern for this film is displayed in Fig. 7.8. A strong series of (00*L*) peaks indicates that the film is predominantly c-axis oriented. However, the appearance of the (110) and (220) peaks shows that the c-axis texturing is not complete. An x-ray ϕ-scan taken for this film is featureless, indicating that there is no in-plane texture in the YBCO film. This is as expected, as the YBCO grows epitaxially on the YSZ intermediate layer, which was not in-plane textured. Therefore, it is not surprising that the critical current of

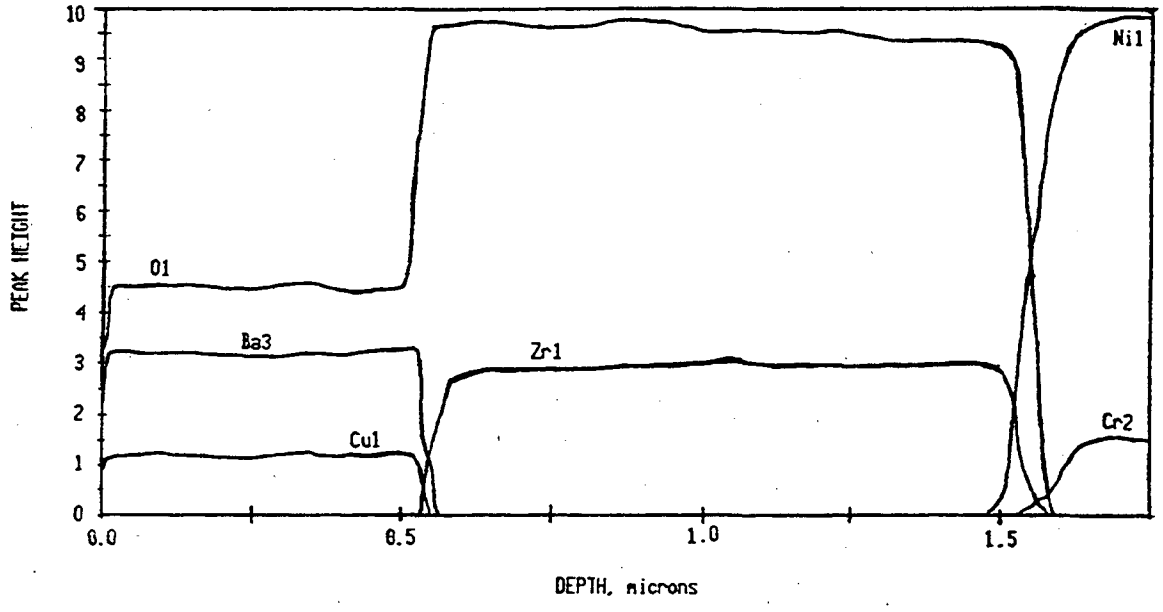

Figure 7.7. Auger elemental depth profile for a YBCO film deposited on a HA230 substrate with a YSZ intermediate layer.

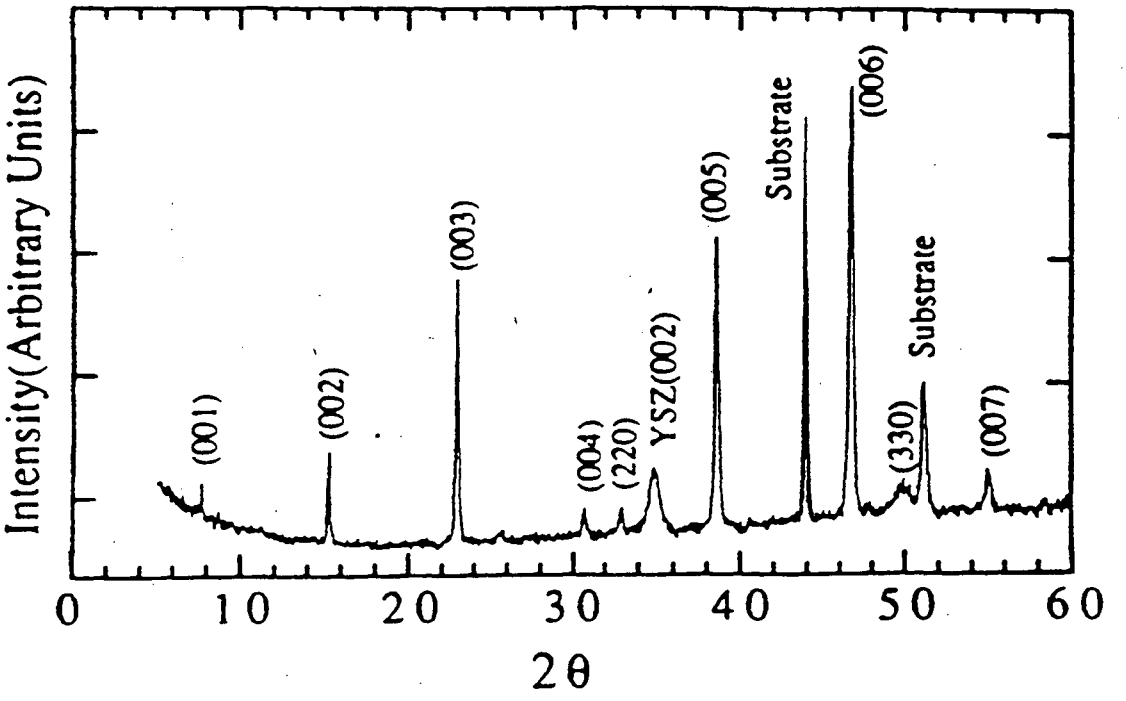

Figure 7.8. X-ray diffraction pattern for a YBCO film deposited on HA230 with a YSZ intermediate layer.

this film is only $J_C \sim 3x10^3$ A/cm^2, well below the values reported for YBCO deposited on YSZ layers that grow epitaxially on Si. To improve the quality of YBCO thin films grown on a YSZ intermediate layer, the control of the YSZ orientation must be improved.

7.3.2. Ion-Assisted Deposition

Ion-assisted depositions were carried out to investigate the possibility of ion-enhanced texturing, as reviewed in Section 5.2. Oxygen or argon gas was supplied to the ion gun at a rate of 10 sccm. The chamber background pressure was held at 1.0 mTorr, as in previous (001) YSZ depositions. For depositions using argon as the ion-beam gas, a total pressure of 1.0 mTorr was achieved by first flowing argon through the gun and adjusting the pumping rate to give a pressure of 0.5 mTorr, and then admitting oxygen through the variable leak valve to 1.0 mTorr. The gun was placed 5-8 cm from the substrate. All other deposition parameters remained the same, though the temperature typically increased from 70 to about 130 °C during a 15 min. deposition due to ion-beam heating.

7.3.2.1. Orientation control

For (001) cubic-YSZ, the [111] channeling direction is 54.7° from the [001] normal direction. According to the results of the previous studies of ion-assisted control of thin film orientation reviewed in Section 5.2, the greatest degree of control is achieved by ion bombardment at an angle corresponding to a channeling direction for the desired orientation. Therefore, the ion gun was positioned at an angle of approximately 55° to the substrate normal.

An XRD pattern from a YSZ film grown with oxygen-ion assistance is shown in Fig. 7.9, with the pattern from a film deposited using the same conditions but without ion-assistance. The ion-beam voltage for this deposition was 100 V and the ion current was 10 mA. Considering that the films are of similar thickness, strongly enhanced (001) texturing is evident. Also, there is no evidence of any unwanted (111) or (011) texture. Variation of the ion-beam angle showed that the greatest enhancement of (001) orientation occurred at the expected angle of 55°, although some texture improvement was seen at all angles from 30 to 60°. These results indicate that ion-assisted control of orientation similar to that for other materials and processes occurs for PLD of YSZ.

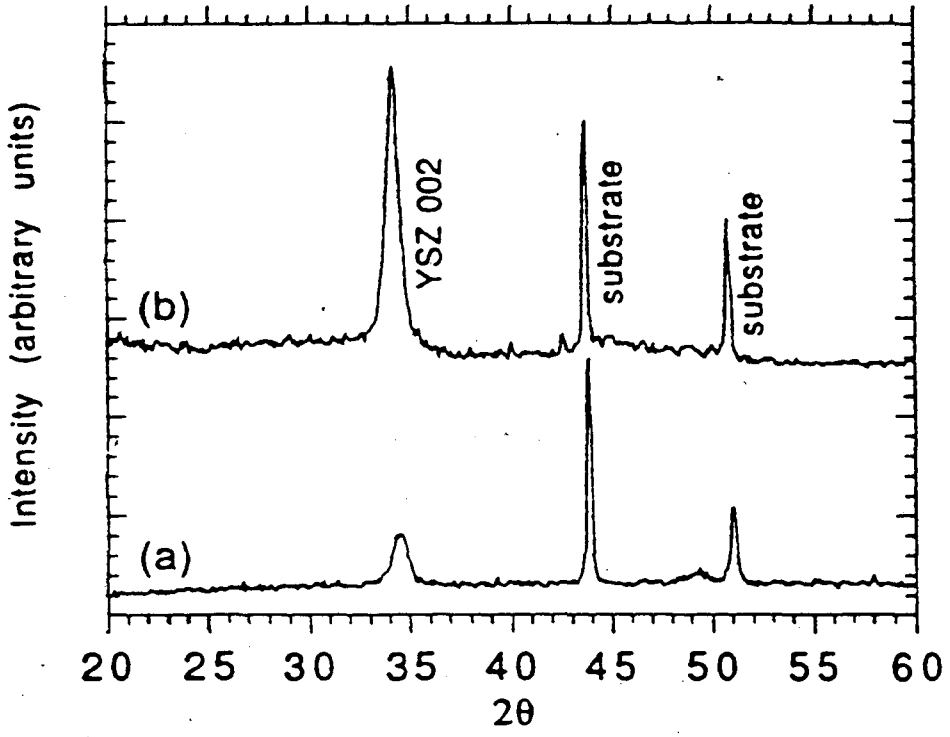

Figure 7.9. X-ray diffraction pattern for YSZ layers deposited on HA230 (a) without and (b) with ion-beam assistance.

7.3.2.2. Ar^+ versus O_2^+ effects

ϕ-scans of films grown with O_2^+ beams showed that although the desired (001)-normal texture was achieved, there was no evidence of any alignment of the in-plane crystal axes. Therefore, subsequently deposited YBCO films did not exhibit in-plane grain alignment, again allowing the existence of a large percentage of high-angle boundaries. This problem limited the YBCO J_c to 10^4 A/cm^2, despite enhanced c-axis normal-texture.

All other publications of ion-enhanced thin film orientation report using argon as the ion-source gas. We initially used oxygen in order to keep all process parameters the same as our non-ion-assisted depositions, while adding ion bombardment. Unlike O_2^+, Ar^+ is non-reactive, and these ions are much different in size and mass. Also, O_2^+ may dissociate immediately upon striking a surface. Therefore, the use of Ar^+ rather than O_2^+ would be expected to change the energetics of the ion-assisted growth.

A YSZ film was deposited using the same process as above but replacing the O_2^+-beam with an Ar^+-beam. An XRD pattern for this film is nearly identical to the one shown in Fig. 7.9(b) for the oxygen-ion-assisted film. However, in contrast to the results for the oxygen-ion-assisted film, the

argon-ion-assisted layer exhibits in-plane texture. This is demonstrated by the (111) ϕ-scan shown in Fig. 7.10, for a YSZ film grown using a 175 V, 10 mA Ar^+-beam. Clear fourfold symmetry confirms a large degree of alignment of the in-plane axes. Also, it should be noted that a peak of (111) intensity in the ϕ-scan occurs at the angle corresponding to the incoming ion direction. This further supports the supposition that control of YSZ film orientation is achieved by ion bombardment along the [111] channeling direction, similar to the results and theories discussed in Section 5.2.

7.3.2.3. Beam voltage effects

In order to determine the effects of beam voltage on the texturing of YSZ, a series of films was deposited by Ar^+-assisted PLD at voltages from 50 to 200 V. Fig. 7.11 shows representative x-ray pole figures from depositions at 50, 100, and 200 V. (In a pole figure the sample is rotated as in a ϕ-scan. In addition, the sample is rocked to measure grain tilt. This is represented by the radial axis in the pole figure.) At 50 V, only slight texturing is evident from the barely-discernible fourfold symmetry. The pole figures for 100 and 200 V beams indicate that the in-plane texture increases with each increase of the beam

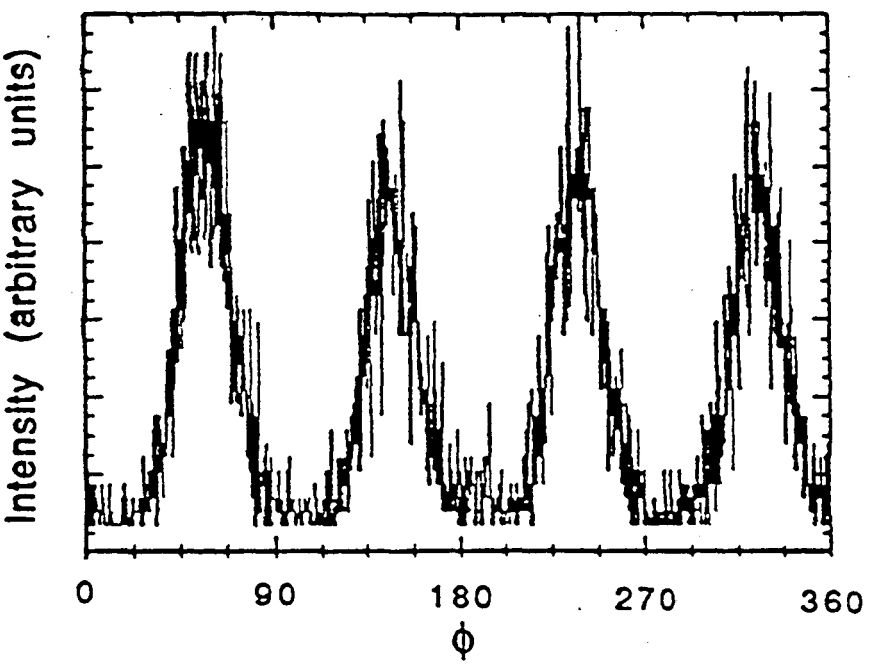

Figure 7.10. (111) ϕ-scan for a YSZ layer grown with Ar^+-beam assistance.

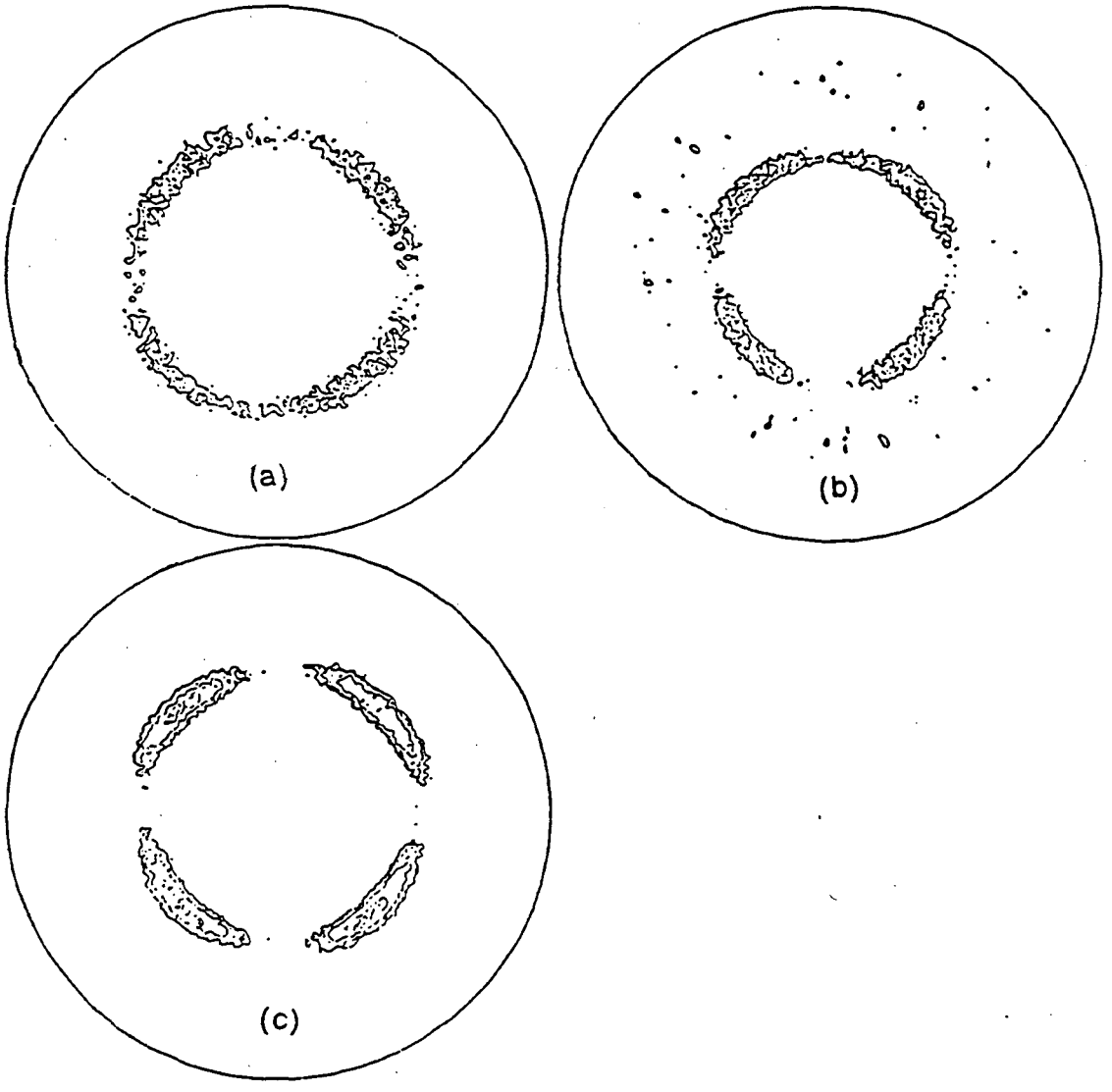

Figure 7.11. YSZ pole figures for ion-assisted deposition beam voltages of: (a) 50V, (b) 100V and (c) 200V.

voltage. With the process conditions used in these depositions and the configuration of the ion gun, 200 V was the highest beam voltage obtainable. Further work is underway to investigate the possibility of even greater in-plane orientation enhancement at higher voltages.

7.3.2.4. Beam current effects

Ion-assisted depositions using ion currents from 5 to 60 mA were conducted. The current was found to have no discernible effect on the degree of YSZ film texture. It was determined that the greatest effect of beam current was to change the deposition rate. At 60 mA, the YSZ growth rate was reduced to near zero, as the rate of beam sputtering of the growing film approached the non-ion-assisted film growth rate. Reduction of the growth rate also occurred as the beam voltage was increased, as would be expected, but the effect of the current was far greater.

From the results described in the previous sections, a summary of the best ion-assisted PLD process conditions for growth of in-plane-textured (001) YSZ is contained in Table 7.2. The film growth rate using these conditions is approximately 0.5 Å/pulse - a 2000-2500 Å film is deposited in 15 min.

Process Parameter	Value
pulse energy density	2 J/cm^2
pulse rate	5 Hz
pressure	1.0 mTorr
temperature	70 °C
target-substrate spacing	4-5 cm
ion-beam gas	Ar^+
ion-beam angle	55°
ion-beam voltage	200 V
ion-beam current	10-20 mA

Table 7.2. YSZ Ion-Assisted PLD Process Parameters

7.3.3. Deposition on Other Substrates

In order to test the applicability of ion-assisted PLD of YSZ on other substrates, single depositions on amorphous silica-glass, alumina, and Teflon substrates were carried out using the same process. The XRD pattern for the YSZ on silica, shown in Fig. 7.12, demonstrates the applicability of this process to grow controlled (001)-oriented YSZ films on other substrates. Although the silica was cut from polished substrate material, the alumina and the Teflon were taken from rough, unpolished materials, and were not prepared in any way other than the usual cleaning. The alumina was

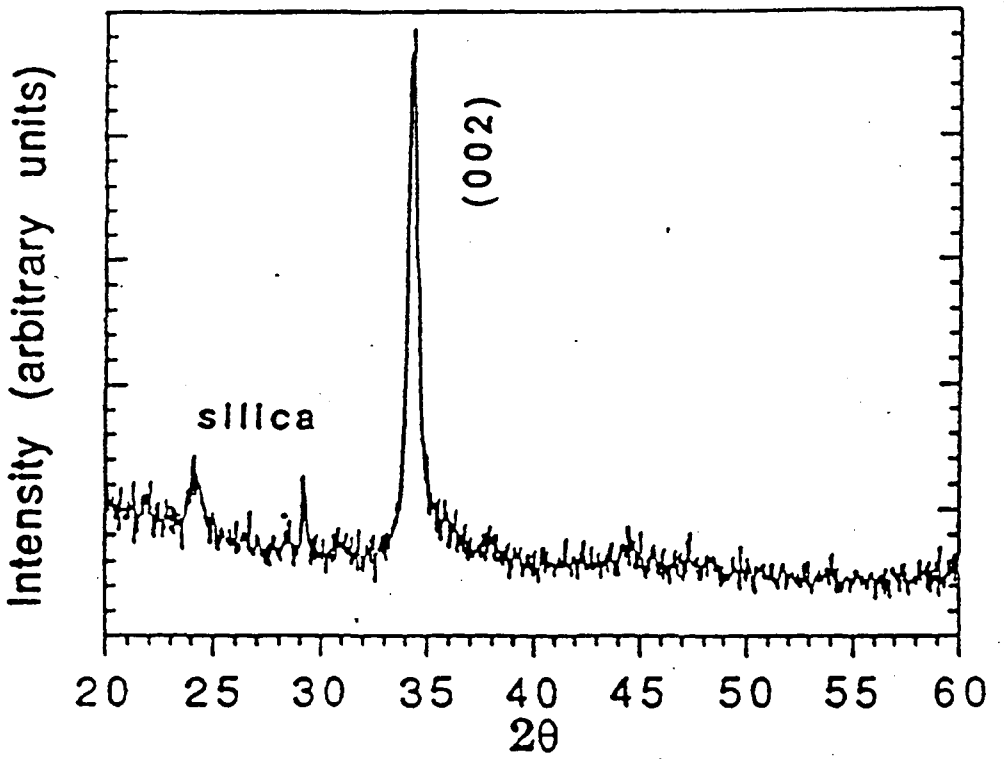

Figure 7.12. X-ray diffraction pattern for a YSZ layer grown with ion-assistance on amorphous silica.

a randomly-oriented polycrystalline substrate. (001) YSZ growth occurred on these substrates as well. X-ray ϕ-scans for the films on silica and alumina are displayed in Fig. 7.13. In-plane texturing is very apparent for both of these films. Though deposition on these substrates was not in any way optimized, these results clearly demonstrate the applicability of this process to a wide variety of substrate materials.

7.4. $YBa_2Cu_3O_{7-\delta}$ Deposition on YSZ-coated Haynes Alloy #230

A 0.4 μm YBCO thin film was deposited on an in-plane-textured (001) YSZ intermediate layer on HA230. The processes used were those detailed in Tables 7.1 and 7.2. The deposition of both layers was carried out *in situ*; i.e., the YSZ and YBCO films were deposited sequentially without opening the deposition chamber.

The 2θ XRD pattern for the YBCO film deposited on the IAPLD-grown YSZ layer is displayed in Fig. 7.14. This scan shows the film to be highly c-axis oriented, with no evidence of other orientations. In fact, the YBCO (00*L*) peak intensities for this film are more than an order of magnitude greater than for films on YSZ layers deposited without ion-

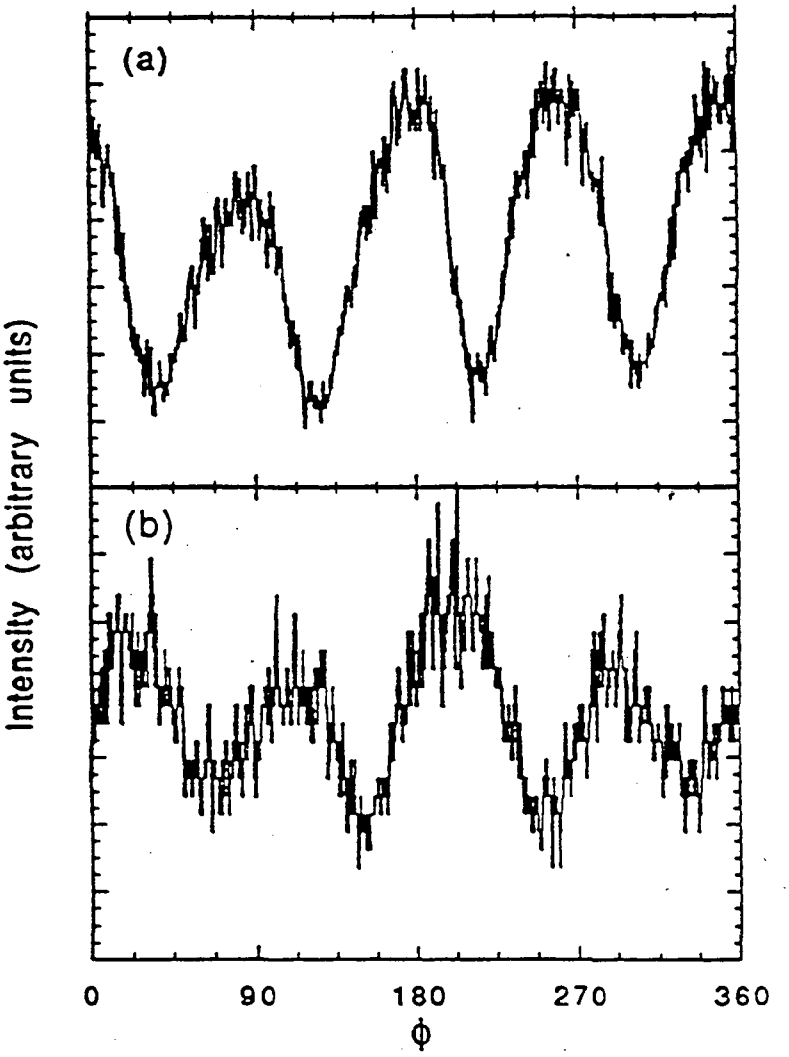

Figure 7.13. (111) YSZ ϕ-scans for ion-assisted deposition on (a) silica, and (b) polycrystalline alumina.

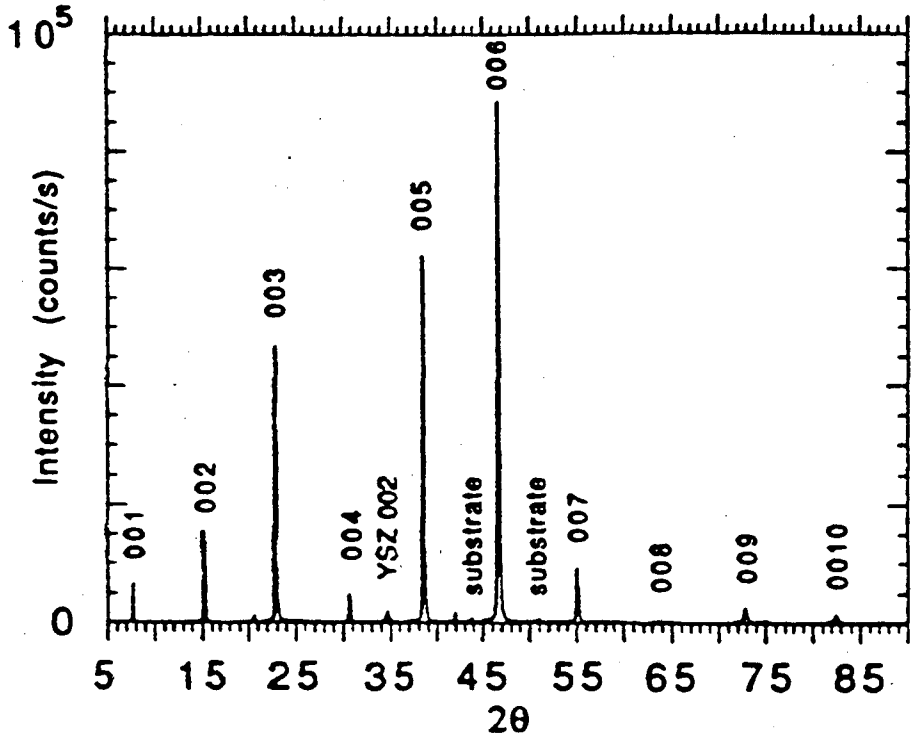

Figure 7.14. X-ray diffraction pattern for a YBCO thin film deposited on a YSZ layer grown with ion-assistance.

assistance, indicating a large improvement in c-axis alignment. A (005) rocking curve measurement found $\Delta\omega \sim 1.3°$ full-width-half-maximum, only slightly higher than for best reported for YBCO thin films on epitaxial YSZ on single-crystal silicon (0.6-1.0°) [40].

A YBCO (103) ϕ-scan for this film is shown in Fig. 7.15. A high degree of in-plane texture is evident, with strong fourfold symmetry of the (103) peak and a low background level. This proves that the growth of the YBCO on the YSZ intermediate layer is indeed epitaxial, with the controlled orientation of the YSZ dictating the properties of the YBCO orientation.

The superconducting properties of the YBCO thin film deposited on the in-plane-aligned YSZ were found to be significantly improved. The T_C is approximately 92 K. Critical current densities as a function of temperature, with and without a 0.4 T magnetic field applied, are shown in Fig. 7.16. The J_C(77K) without field is 6×10^5 A/cm^2, while with field parallel and at 45° (the field direction for which J_C is lowest), the J_C's fall to 8×10^4 and 3×10^4 A/cm^2 respectively. These values are higher than any others reported for YBCO films deposited on randomly-oriented polycrystalline substrates or other substrates on which YBCO does not grow

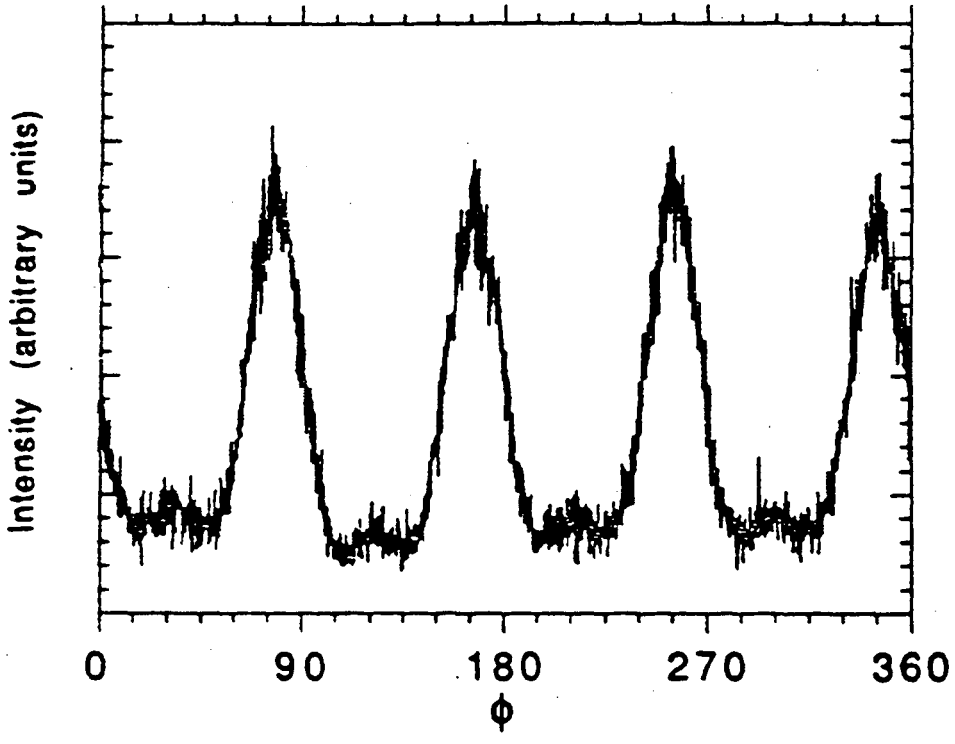

Figure 7.15. (103) YBCO ϕ-scan for a film deposited on a YSZ layer grown with ion-assistance.

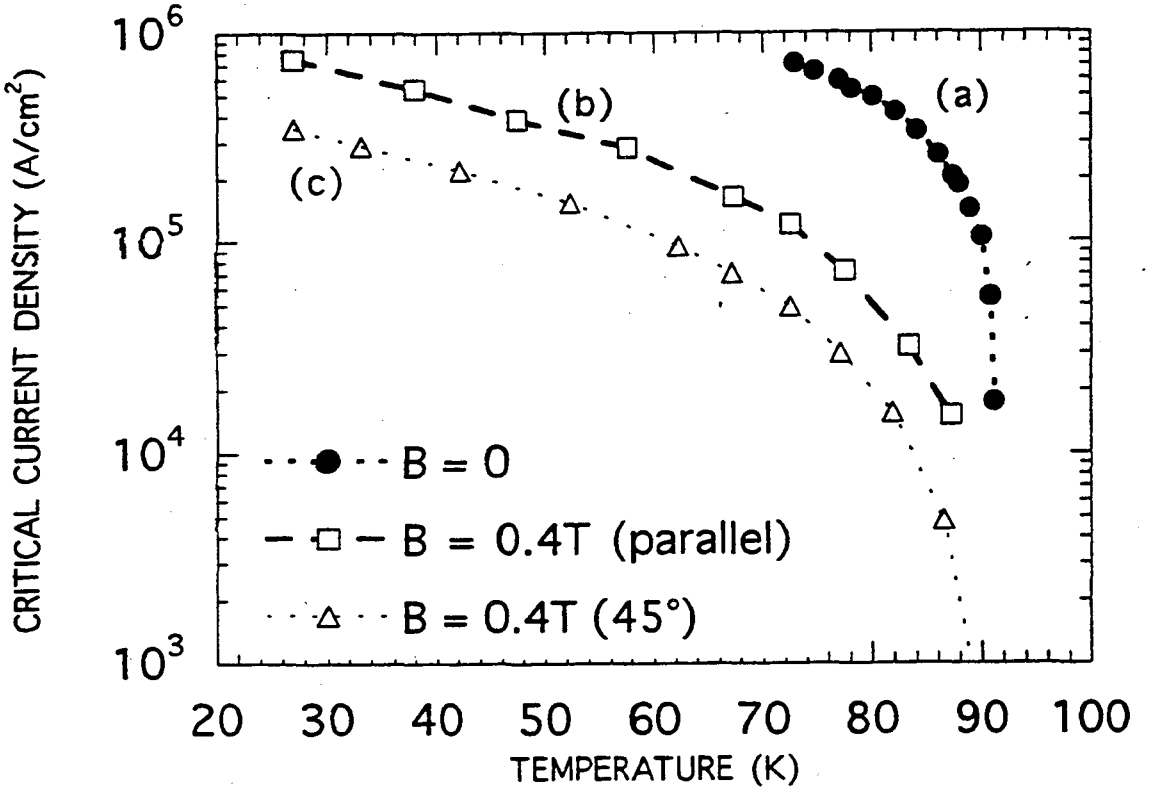

Figure 7.16. YBCO critical current densities (a) without magnetic field, and with a 0.4T field (b) parallel to the film and (c) 45° to the film normal, the field direction for which J_C is lowest.

epitaxially. In fact, the current-carrying capacity of this film is not far from that of the best epitaxial films on silicon with an epitaxial YSZ intermediate layer, $J_C(77K) \sim 2x10^6$ A/cm^2 [40].

8. DISCUSSION

8.1. $YBa_2Cu_3O_{7-\delta}$ Thin Film Results and Potential

The critical current densities achieved in this work for YBCO thin films are the highest reported for the growth of YBCO on a substrate on which direct epitaxial growth is not possible. It is in fact quite remarkable that it is now possible to control the textured growth of a structure as complex as YBCO on a randomly-oriented metal alloy substrate. However, there may yet be room for a great deal of improvement through a further understanding and optimization of the processing techniques developed here. To justify this statement, I refer to Fig. 7.15, the YBCO ϕ-scan for the best film. It is clear from this scan that there is still a significant degree of in-plane grain misalignment in this film. This is evidenced by both the baseline level in the scan, which represents randomly aligned material, and the width

of the peaks, which show that the material that we have referred to as aligned is in reality as much as ~ 30 degrees misaligned. This is a consequence of the misalignment contained in the IAPLD-deposited YSZ intermediate layer that serves as the template for YBCO growth. Improvement of the texture of this layer is quite likely with further characterization of the deposition process, as only a very narrow range of process conditions has been investigated thus far. In particular, in Section 7.3.2.3 it was noted that our system was limited to an ion beam voltage of 200 V. Up to this voltage, our results show a strong improvement in the in-plane alignment with increasing voltage. Thus, I anticipate that further improvement is likely to be possible with further increases in beam voltage.

The potential of the results achieved here for the manufacture of YBCO superconducting tapes, the original purpose of this work, is demonstrated by comparing these results to the results for competing technologies. The most widely studied approach to developing current-carrying high-temperature superconductor wires is the so-called "Bi-powder-in-tube" technique. A silver tube is filled with Bi-Sr-Ca-Cu-O, and then subjected to processing to crystallize and texture the superconducting material. K. Sato *et al.* at

Sumitomo [103], whose work is considered the benchmark for this technology, have reported critical current densities (77K) of 4.7×10^4 A/cm^2 without applied magnetic field, and 1×10^4 A/cm^2 with a 1.0 T field applied. These results are plotted in Fig. 8.1, with the results af our work, and recent results for thick film deposition of the Tl-Ca-Ba-Cu-O superconductor using a spray coating technique [104]. For reference, the critical current density versus magnetic field for a YBCO film on single-crystal YSZ is shown. It is clear that we have achieved much higher critical current densities than has been demonstrated for competing technologies.

8.2. Applicability of Demonstrated Technology

The control of thin film orientation using ion-assisted pulsed-laser deposition that has been investigated herein may be applicable to a wide range of thin film technologies, both within the field of high-temperature superconductors and in other areas. Another application for high-temperature superconductors that we are aware of is the use of YBCO thin films in a multi-chip module, currently being developed by the Advanced Research Projects Administration. In this module, at least

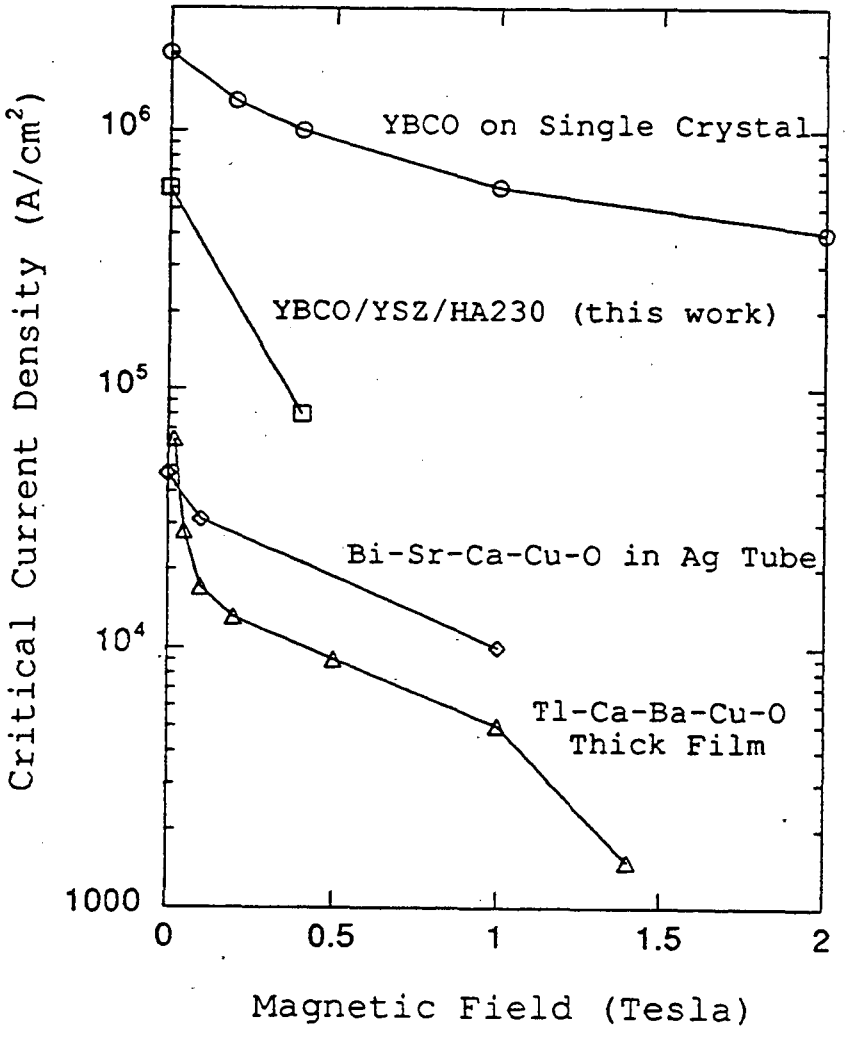

Figure 8.1. A comparison of the critical current densities (77K) as a function of magnetic field for different high-temperature superconducting wire technologies [Refs. 19, 103, 104]. Data for a YBCO film deposited on a YSZ single-crystal substrate is shown for reference. (Lines are drawn for guidance only.)

three separate layers of YBCO are needed: the first as a ground plane and the others for interconnects between the modules. These layers must have high current capacity and must be separated by insulating layers. Currently, the only way to achieve this is to maintain an epitaxial relationship from a single crystal substrate, up through each successive layer, including the insulating layers. Needless to say, this is very difficult and puts severe constraints on the insulating layer, which must be lattice-matched with the substrate and YBCO. In most applications, such as the common use of SiO_2 layers as insulators in the semiconductor industry, amorphous insulating layers are employed. With the technology demonstrated here, amorphous insulating layers could be used between the YBCO layers, as long as a IAPLD-grown YSZ layer is deposited before each YBCO layer to provide *c*-axis crystalline growth. Also, this would remove the requirement that the substrate be a single crystal, as a single crystal template would no longer be needed.

The applicability of this technology may extend well beyond superconductor thin films. For example, in the manufacture of silicon microelectronic components such as processors and

memory chips, a variety of thin films are deposited to provide interconnects between devices and insulating layers. With present technology, these layers must be either amorphous or randomly-oriented polycrystalline material. This is dictated by the fact that an amorphous SiO_2 layer is typically grown to isolate the silicon devices from the layers above. However, with the IAPLD technique developed here, oriented crystalline films could be deposited at any point in the manufacturing process. Perhaps even an additional semiconductor device layer could be grown, though the quality of this layer could obviously not be the same as the single crystal substrate. This could open up new possibilities in microelectronic design.

8.3. Mechanism of YSZ Orientation Control by Ion-Assisted Pulsed-Laser Deposition

One of the most important questions that this research was to answer is "Is it possible to control the orientation of a YSZ thin film grown on a randomly-oriented metal alloy substrate using an ion-assisted pulsed-laser deposition process?" The first answer that was needed was whether or not the results and models of others for the ion-assisted

orientation effects applied to the pulsed-laser deposition technique whatsoever. As was discussed in Section 5, PLD is a pulsed process, resulting in a non-continuous arrival of material at the growth surface. All previous studies of ion-assisted orientation control used continuous deposition methods, such as sputtering. Since ion sources provide continuous ion beams, we were not sure that IAPLD would yield similar control of orientation. However, from the results in Section 7 showing clear alignment of the YSZ in-plane axes with the addition of ion bombardment, it is quite certain that this method works with PLD.

The next part of the question that we sought to answer is "Do our results support the models describing the mechanism of ion-bombardment orientation control put forth by Bradley [94] and others?" First, let us consider whether the effects we have observed are caused by a nucleation or a growth phenomenon. Bradley models the mechanism as a continuous selection process **during film growth** due to the difference in sputtering rates for film grains with a channeling direction parallel to the ion bombardment direction and those without such alignment. In fact, one of the assumptions of Bradley's model is that the nucleation of the film on the substrate is a random

process that is unaffected by the ion bombardment. Our results agree with this model. We have found that we can grow YSZ films with similar control of orientation on several different substrates: HA230, silica, polycrystalline alumina, and even Teflon. In most thin film experiments, a change of substrate strongly influences the film nucleation characteristics. The fact that our films grown on such widely different substrates have similar characteristics supports the idea that the nucleation step is unimportant to the control of orientation in IAD.

Further evidence that the control of orientation is caused by a growth-related mechanism rather than a nucleation effect was obtained by depositing the following three films on HA230 (using the process in Table 7.2): (1) ion bombardment started **before** the laser deposition; (2) ion bombardment and laser deposition started **simultaneously**; (3) ion bombardment started **after** 1 min. of laser deposition (~ 30 nm non-ion-assisted film). X-ray diffraction measurements of these three films indicated nearly identical control of orientation by the three processes. If the ion-assisted texture control was affected by the nucleation on the substrate, film #3 would not have had the same characteristics as the other two. We

conclude that, as modeled by Bradley, this is a growth-related mechanism.

Another feature predicted by Bradley's model is that the selection of the preferred orientation by IAD is a gradual process during growth. As each new layer of film grows, the grains in the preferred alignment make up a larger percentage of that layer. This means that the surface of a thicker film should be aligned in the preferred orientation to a greater degree than a thinner film. Unfortunately, this is a difficult phenomenon to measure. Standard x-ray diffraction techniques sample the entire film thickness during measuring, so it is difficult to prove a difference between top and bottom layers. The best way to perform this measurement would be by cross-sectional transmission electron microscopy, which would enable direct imaging of the top and bottom regions of the film. However, this was beyond the scope of this project (see Section 8.4, "Suggestions for Future Work"). We do have one indirect piece of evidence that the top surface of an IAPLD YSZ film is better-aligned than the bulk of the film. A comparison of the x-ray rocking-curve widths as well as the peak widths from the ϕ-scans of the IAPLD YSZ and subsequently deposited YBCO indicate that the YBCO is aligned to a greater

degree than the bulk of the YSZ. As noted in Section 7.4, the rocking-curve width, a measure of the planar tilt in the film, of the YBCO film is $\Delta\omega \sim 1.3°$. What was not mentioned was that the YSZ measurement found $\Delta\omega \sim 4°$, showing that the YBCO film is better than the bulk of the underlying YSZ. Also, a comparison of the widths of the ϕ-scan peaks in Figs. 7.10 and 7.15 finds that the peak for YSZ is ~ 5° wider than that for YBCO. This shows that the range of grain alignment is narrower in the YBCO than in the YSZ. If we assume that the YBCO alignment is dictated by epitaxy on the surface of the YSZ, then the YSZ surface must be better-aligned than the bulk of the film. Though this evidence is not conclusive, it does support the agreement between these results and Bradley's model derived from other systems.

Finally, we ask whether or not the results of our investigations of the effects of beam parameters support the IAD mechanism models. First, our results determined that the greatest degree of alignment occurred with the angle of ion incidence ~ 55° from the film normal. This corresponds to the [111] channeling direction in YSZ, and therefore strongly supports the models of Bradley and Dobrev. Second, we showed in Section 7.3.2.3 that the control of orientation for our YSZ

films increased with increasing ion-beam voltage. As the models are based on differences in the energy transfer process caused by the alignment or misalignment of channeling axes to the ion beam, one might predict that using higher ion energies would accentuate the differences. Our results support this idea. Lastly, we determined that changing the ion-beam current affected only the growth rate, not the alignment control. This is logical, since the ion energy is not changed in this experiment, only the rate of arrival. This would not be expected to change the ratio of the sputtering rates of the aligned and misaligned material; only the overall rate should be affected. Thus, we once again conclude that our results conform well to the ion-assisted orientation control model of Bradley.

8.4. Suggestions for Future Research

As is probably the case for any study such as this that explores an entirely new area of technology, this work has perhaps identified more questions than it has provided answers. There are too many avenues for future research than can be listed here, but a few important ideas should be presented, many of which have already been

mentioned in this work. First, a very narrow range of process parameters has been investigated so far for the YSZ IAPLD process. It was already noted that our beam voltage was limited by our system configuration. This problem is in the process of being overcome by the purchase and installation of a new ion gun, along with modifications to the system. Besides the beam voltage, other parameters that are in particular need of more study are the process pressure, flow rates, and gas environment.

Another investigation that would likely provide valuable information is cross-sectional transmission electron microscopy (TEM). TEM imaging of a YSZ film throughout its thickness should provide direct evidence of the predicted increased preferred orientation alignment with film thickness. Understanding the degree to which the alignment improves with increasing thickness would help determine the optimal thickness for the YSZ layer. Perhaps much greater alignment is possible for much thicker films than have been considered thus far.

Once the optimal process parameters are determined and the issue of optimal thickness addressed, it then would be extremely interesting to determine the ultimate YBCO critical current density that can be produced by this technology.

It is entirely conceivable that values approaching those achieved on single-crystal silicon with YSZ buffer layers could be obtained or even exceeded.

Finally, our results are the first to point out that a single process provides films with controlled orientation on several different substrates. This investigation should be expanded to include different film materials as well as substrates. Can we align any thin film we want on any substrate on which epitaxy does not dictate the orientation? This would certainly be exciting, and could have a significant impact on the future of thin film growth. Of particular interest for high-temperature superconductors would be the controlled orientation of films of $SrTiO_3$, CeO_2, and MgO, among others. Other films might be of interest for other technologies.

REFERENCES

1. Bednorz, J.G. & Muller. *Z. Phys. B* **64**, 189 (1986).
2. Wu, M.K., Ashburn, J.R., Torng, C.J., Hor, P.H., Meng, R.L., Gao, L., Huang, Z.J., Wang, Y.Q. & Chu, C.W. *Phys. Rev. Lett.* **58**, 908 (1987).
3. Larbalestier, D.C., ed. *Applications of High T_C Superconductivity* in *MRS Bulletin* **17**(8) (1992).
4. Van Duzer, T. & Turner, C.W. *Principles of Superconductive Devices and Circuits* (Elsevier, New York, 1981).
5. Yu, L.S., Harper, J.M.E., Cuomo, J.J. & Smith, D.A. *Appl. Phys. Lett.* **47**, 932 (1985).
6. Maeda, H., Tanaka, Y., Fukutomi, M. & Asano, T. *Jpn. J. Appl. Phys.* **27**, L209 (1988).
7. Sheng, Z.Z. & Hermann, A.M. *Nature* **332**, 138 (1988).
8. Schilling, A., Cantoni, M., Guo, J.D. & Ott, H.R. *Nature* **363**, 56 (1993).
9. Dijkkamp, D., Venkatesan, T., Wu, X.D., Shaheen, S.A., Jisrawi, N., Min-Lee, Y.H., McLean, W.L. & Croft, M. *Appl. Phys. Lett.* **51**, 619 (1987).

10. Barrett, C.R., Nix, W.D. & Tetelman, A.S. *The Principles of Engineering Materials* (Prentice-Hall, Englewood Cliffs, 1973).

11. Kittel, C. *Introduction to Solid State Physics* (John Wiley & Sons, New York, 1986).

12. Schuller, I.K. & Jorgensen, J.D. *MRS Bulletin* **14**(1), 27 (1989).

13. Sleight, A.W. *Science* **242**, 1519 (1988).

14. Cava, R.J., Batlogg, B., Chen, C.H., Rietman, E.A., Zahurak, S.M. & Werder, D. *Phys. Rev. B* **36**, 5719 (1987).

15. Tarascon, J.-M., Barboux, P., Bagley, B.G., Greene, L.H., McKinnon, W.R. & Hull, G.W. in *Chemistry of High Temperature Superconductors* (eds. Nelson, D.L., Whittingham, M.S. & George, T.F.) 198 (American Chemical Society, Washington, DC, 1987).

16. Markert, J.T., Dunlap, B.D. & Maple, M.B. *MRS Bulletin* **14**(1), 37 (1989).

17. Dimos, D., Chaudhari, P. & Mannhart, J. *Phys. Rev. B* **41**, 4038 (1990).

18. Ivanov, Z.G., Nilsson, P.A., Winkler, D., Alarco, J.A., Claeson, T., Stepantsov, E.A. & Tzalenchuk, A.Y. *Appl. Phys. Lett.* **59**, 3030 (1991).

19. Norton, D.P., Lowndes, D.H., Budai, J.D., Christen, D.K., Jones, E.C., Lay, K.W. &

Tkaczyk, J.E. *Appl. Phys. Lett.* **57**, 1164 (1990).

20. Oda, Y., Fujita, H., Toyoda, H., Kaneko, T., Kohara, T., Nakada, I. & Asayama, K. *Jpn. J. Appl. Phys.* **26**, L1660 (1987).
21. Xiao, G., Cieplak, M.Z., Gavrin, A., Streitz, F.H., Bakhshai, A. & Chien, C.L. *Phys. Rev. Lett.* **60**, 1446 (1988).
22. Shimakawa, Y., Kubo, Y., Utsumi, K., Takeda, Y. & Takano, M. *Jpn. J. Appl. Phys.* **27**, L1071 (1988).
23. Cheung, C.T. & Ruckenstein, E. *J. Mater. Res.* **4**, 1 (1989).
24. Venkatesan, T., Wu, X.D., Dutta, B., Inam, A., Hegde, M.S., Hwang, D.M., Chang, C.C., Nazar, L. & Wilkens, B.J. *Appl. Phys. Lett.* **54**, 581 (1989).
25. Koren, G. & Gupta, A. *Appl. Phys. Lett.* **54**, 1920 (1989).
26. Busch, H., Fink, A. & Muller, A. *J. Appl. Phys.* **70**, 2449 (1991).
27. Roas, B., Endres, G. & Schultz, L. *Appl. Phys. Lett.* **53**, 1557 (1988).
28. Ramesh, R., Inam, A., Hwang, D.M., Ravi, T.S., Sands, T., Xi, X.X., Wu, X.D., Li, Q., Venkatesan, T. & Kilaas, R. *J. Mater. Res.* **6**, 2264 (1991).

29. Singh, R.K., Narayan, J., Singh, A.K. & Krishnaswamy, J. *Appl. Phys. Lett.* **54**, 2271 (1989).

30. Chan, S.W., Chase, E.W., Wilkens, B.J. & Hart, D.L. *Appl. Phys. Lett.* **54**, 2032 (1989).

31. Mogro-Campero, A., Turner, L.G., Hall, E.L., Garbauskas, M.F. & Lewis, N. *Appl. Phys. Lett.* **54**, 2719 (1989).

32. Lee, S.G., Koren, G., Gupta, A., Segmuller, A. & Chi, C.C. *Appl. Phys. Lett.* **55**, 1261 (1989).

33. Moeckly, B.H., Russek, S.E., Lathrop, D.K., Buhrman, R.A., Li, J. & Mayer, J.W. *Appl. Phys. Lett.* **57**, 1687 (1990).

34. Lee, W.Y., Salem, J., Lee, V., Huang, T., Savoy, R., Deline, V. & Duran, J. *Appl. Phys. Lett.* **52**, 2263 (1988).

35. Nakajima, H., Yamaguchi, S., Iwasaki, K., Morita, H., Fujimori, H. & Fujino, Y. *Appl. Phys. Lett.* **53**, 1437 (1988).

36. Venkatesan, T., Chase, E.W., Wu, X.D., Inam, A., Chang, C.C. & Shokoohi, F.K. *Appl. Phys. Lett.* **53**, 243 (1988).

37. Mogro-Campero, A. *Supercond. Sci. Technol.* **3**, 155 (1990).

38. Tate, J., Berberich, P., Dietsche, W. & Kinder, H. *Less-Common Met.* **151**, 311 (1989).

39. Lee, J.-W., Schlesinger, T.E., Stamper, A.K., Migliuolo, M., Greve, D.W. & Laughlin, D.E. *J. Appl. Phys.* **64**, 6502 (1988).

40. Fork, D.K., Fenner, D.B., Barton, R.W., Phillips, J.M., Connel, G.A.N., Boyce, J.B. & Geballe, T.H. *Appl. Phys. Lett.* **57**, 1161 (1990).

41. Jia, Q.X. & Anderson, W.A. *Appl. Phys. Lett.* **57**, 304 (1990).

42. Tiwari, P., Kanetkar, S.M., Sharan, S. & Narayan, J. *Appl. Phys. Lett.* **57**, 1578 (1990).

43. Wittanachchi, S., Patel, S., Kwok, H.S. & Shaw, D.T. *Appl. Phys. Lett.* **54**, 578 (1989).

44. Chang, L.D., Tseng, M.Z., Hu, E.L. & Fork, D.K. *Appl. Phys. Lett.* **60**, 1753 (1992).

45. Heuer, A.H. & Hobbs, L.W. *Science and Technology of Zirconia* (American Ceramic Society, Columbus, 1981).

46. Claussen, N., Ruhle, M. & Heuer, A.H. *Science and Technology of Zirconia II* (American Ceramic Society, Columbus, 1984).

47. Ray, M.A., Greene, J.E., Polack, A.J. & Welsh, L.B. *J. Vac. Sci. Technol.* **A1**, 322 (1983).

48. Filby, J.D. & Nielsen, S. *Brit. J. Appl. Phys.* **18**, 1537 (1967).

49. Legagneux, P., Gary, G., Dieumegard, D., Schwebel, C., Pellet, C., Gautherin, G. & Siejka, J. *Appl. Phys. Lett.* **53**, 1506 (1988).

50. Fukumoto, H., Imura, T. & Osaka, Y. *Jpn. J. Appl. Phys.* **27**, L1404 (1988).

51. Stubican, V.S., Hink, R.C. & Ray, S.P. *J. Am. Ceram. Soc.* **61**, 17 (1978).

52. Wagner, C. *Naturwissenschaften* **31**, 265 (1943).

53. Hund, F. *Z. Phys. Chem.* **199**, 142 (1952).

54. Rhodes, W.H. & Carter, R.E. *J. Am. Ceram. Soc.* **49**, 244 (1966).

55. Simpson, L.A. & Carter, R.E. *J. Am. Ceram. Soc.* **49**, 139 (1966).

56. Ruh, R. & Garrett, H.J. *J. Am. Ceram. Soc.* **50**, 257 (1967).

57. Heuer, A.H. & Ruhle, M. in Ref. 45.

58. Morinaga, M., Adachi, H. & Tsukuda, M. *J. Phys. Chem. Solids* **44**, 301 (1983).

59. Tietz, L.A., Carter, C.B., Lathrop, D.K., Russek, S.E., Buhrman, R.A. & Michael, J.R. *J. Mater. Res.* **4**, 1072 (1989).

60. Norton, D.P., Lowndes, D.H., Budai, J.D., Christen, D.K., Jones, E.C., McCamy, J.W., Ketcham, T.D., St. Julien, D., Lay, K.W. & Tkaczyk, J.E. *J. Appl. Phys.* **68**, 223 (1990).

61. Garrison, S.M., Newman, N., Cole, B.F., Char, K. & Barton, R.W. *Appl. Phys. Lett.* **58**, 2168 (1991).

62. Fork, D.K., Garrison, S.M., Hawley, M. & Geballe, T.H. *J. Mater. Res.* **7**, 1641 (1992).

63. Fork, D.K., Fenner, D.B., Connell, G.A.N., Phillips, J.M. & Geballe, T.H. *Appl. Phys. Lett.* **57**, 1137 (1990).

64. Smith, H.M. & Turner, A.F. *Appl. Opt.* **4**, 147 (1965).

65. Beech, F. & Boyd, I.W. in *Photochemical Processing of Electronic Materials* (eds. Boyd, I.W. & Jakman, R.B.) 387 (Academic Press, New York, 1991).

66. Hubler, G.K., ed. *Pulsed Laser Deposition* in *MRS Bulletin* **17**(2) (1992).

67. Singh, R.K. & Narayan, J. *Phys. Rev. B* **41**, 8843 (1990).

68. von Allmen, M. *Laser-Beam Interactions with Materials: Physical Principles and Applications* (Springer, New York, 1987).

69. Cheung, J. & Horwitz, J. *MRS Bulletin* **17**(2), 30 (1992).

70. Ready, J.F. *Effects of High Power Laser Radiation* (Academic Press, New York, 1971).

71. Mao, X.L., Chan, W.T., Shannon, M.A. & Russo, R.E. *J. Appl. Phys.* **74**, 4915 (1993).

72. Otis, C.E. & Dreyfus, R.W. *Phys. Rev. Lett.* **67**, 2102 (1991).

73. Neifled, R.A., Potenziani, E., Sinclair, W.R., Hill, W.T., III, Turner, B. & Pinkas, A. *Appl. Phys. Lett.* **69**, 1107 (1991).

74. Chan, W.T., Mao, X.L. & Russo, R.E. *Appl. Spectrosc.* **46**, 1025 (1992).

75. Hubler, G.K. *MRS Bulletin* **17**(2), 26 (1992).

76. Ghandi, S.K. *VLSI Fabrication Principles* (John Wiley & Sons, New York, 1983).

77. Kaufman, H.R. *Adv. Electr. Elect. Phys.* **36**, 265 (1974).

78. Kaufman, H.R., Cuomo, J.J. & Harper, J.M.E. *J. Vac. Sci. Technol.* **21**, 725 (1982).

79. Smidt, F.A. *Inter. Mater. Rev.* **35**, 61 (1990).

80. Lewis, B. & Anderson, J.C. *Nucleation and Growth of Thin Films* (Academic Press, New York, 1978).

81. Pranevicius, P. *Nucl. Instrum. Meth.* **182/183**, 251 (1981).

82. Macchioni, C.V. *J. Vac. Sci. Technol.* **A9**, 2302 (1991).

83. Krikorian, E. & Sneed, R.J. *Astrophys. Space Sci.* **65**, 129 (1979).

84. McNally, J.J., Al-Jumaily, G.A., McNeil, J.R. & Bendow, B. *Appl. Opt.* **25**, 1973 (1986).

85. Martin, P.J. *J. Mater. Sci.* **21**, 1 (1986).

86. Martin, P.J., Netterfield, R.P. & Sainty, W.G. *J. Appl. Phys.* **55**, 235 (1984).

87. Marinov, M. *Thin Solid Films* **46**, 267 (1977).

88. Dobrev, D. *Thin Solid Films* **92**, 41 (1982).

89. Messier, R. & Ross, R.C. *J. Appl. Phys.* **53**, 6220 (1982).

90. Choi, C.H., Ramanarayanan, R., Mei, S.N. & Lu, T.M. in *Materials Modification and Growth Using Ion Beams* (ed. Gibson, U.J.) 105 1987).

91. Kay, E., Parmigiani, F. & Parrish, W. *J. Vac. Sci. Technol.* **A6**, 3074 (1988).

92. Kung, K.T.Y. & Reif, R. *J. Appl. Phys.* **59**, 2422 (1986).

93. Wang, P., Thompson, D.A. & Smeltzer, W.W. *Nucl. Instrum. Meth. Phys. Res.* **B7/8**, 97 (1985).

94. Bradley, R.M., Harper, J.M.E. & Smith, D.A. *J. Appl. Phys.* **60**, 4160 (1986).

95. Auciello, O. & Kelly, R. *Ion Bombardment Modification of Surfaces* (Elsevier, New York, 1984).

96. Seitz, F. & Koehler, J.S. *Solid State Phys.* **2**, 307 (1956).

97. Whetten, T.J., Armstead, A.A., Grzybowski, T.A. & Ruoff, A.L. *J. Vac. Sci. Technol.* **A2**, 477 (1984).

98. Snouse, T.W. & Haughney, L.C. *J. Appl. Phys.* **37**, 700 (1966).

99. Morris, D.E., Asmar, N.G., Nickel, J.H., Sid, R.L., Wei, J.Y.T. & Post, J.E. *Physica C* **159**, 287 (1989).

100. Haynes International. *Haynes Alloy #230*, company literature (1989).

101. Cullity, B.D. *Elements of X-Ray Diffraction* (Addison-Wesley, Reading, 1978).

102. Meyers, A.M. *AC Electrical Characterization of High-Temperature Superconducting Thin Films* (Lawrence Berkeley Laboratory, 1989).

103. Sato, K., Shibuta, N., Mukai, H. & Hikata, T. *Physica C* **190**, 50 (1991).

104. DeLuca, J.A., Karas, P.L., Tkaczyk, J.E. & Bednarczyk, P.J. *Physica C* **205**, 21 (1993).

LAWRENCE BERKELEY LABORATORY
UNIVERSITY OF CALIFORNIA
TECHNICAL INFORMATION DEPARTMENT
BERKELEY, CALIFORNIA 94720